Analysis of the creep coefficient of binary sand-bentonite mixtures in oedometer condition using mixture theory

By

X.S. Shi (Corresponding author)

Department of Civil and Environmental Engineering

The Hong Kong Polytechnic University, Hung Hom, Kowloon, Hong Kong.

Email: qingsongsaint@gmail.com

Jianhua Yin

Department of Civil and Environmental Engineering

The Hong Kong Polytechnic University, Hung Hom, Kowloon, Hong Kong, China

Tel: (852) 2766-6065, Fax: (852) 2334-6389, Email: cejhyin@polyu.edu.hk

Weiqiang Feng

Department of Civil and Environmental Engineering

The Hong Kong Polytechnic University, Hung Hom, Kowloon, Hong Kong.

Email: sam.feng@polyu.edu.hk

Wenbo Chen

Department of Civil and Environmental Engineering

The Hong Kong Polytechnic University, Hung Hom, Kowloon, Hong Kong.

Email: wenbo.chen@connect.polyu.hk

Apr. 2018

Abstract

A series of oedometer tests was performed on the binary sand-bentonite mixtures, considering both the effect of sand mass fraction and the initial water content of the bentonite matrix. The experimental data reveals that the influence of initial water content of the bentonite matrix on the overall creep behavior of the mixture is negligible. However, the reference time line (corresponding to 24h of consolidation) is significantly affected by both the initial water content and the sand mass fraction. The local creep parameter of the bentonite matrix is approximately close to that of the pure bentonite for a mixture with a sand mass fraction of 50%. However, it decreases with the further increase of sand mass fraction due to increasing inhomogeneity of the binary mixtures and a formation of clay-bridges between adjacent sand inclusions. An equivalent local creep parameter is defined, and a new structure variable is introduced, which can be approximated by the structure variable responsible for the inter-granular structure evolution. Finally, a creep model was formulated using mixture theory. The proposed model has five parameters, one structure parameter incorporating the inter-granular structure effect, and the others depend on the intrinsic behavior of the pure bentonite. Only two conventional oedometer tests need to be done for calibrating the parameters. The model prediction is then compared with experimental data, revealing a satisfactory performance of the proposed model.

Keywords: Sand-bentonite mixtures; Compressibility; Creep; Homogenization; Inter-granular structure

Introduction

Sand-bentonite mixtures are commonly adopted as a barrier material (Graham *et al.*, 1992; Peters and Berney, 2010; Tong and Yin, 2011; Wang *et al.*, 2013). As a binary mixture, (with coarse sand particles being the inclusions and fine bentonite being the clay matrix), it inherits the property of the bentonite clay matrix, e.g., high swelling potential, low hydraulic conductivity and radionuclide retardation capacity (Sivapullaiah *et al.*, 2000; Vilarrasa *et al.*, 2005; Pal and Ghosh, 2005; Thyagaraj *et al.*, 2016; Deng *et al.*, 2017). The behavior of bentonite depends on its two levels of pore system: intra-aggregate pores inside and between the clay particles in clay aggregates, and inter-aggregate pores between the clay aggregates (Delage *et al.*, 2006; Nowamooz, 2014).

The compressibility of sand-bentonite mixtures can be divided into two parts, one is coupled with the pore water dissipation (primary consolidation), and the other one is creep deformation after the end of primary consolidation. It is widely accepted that a primary consolidation is due to the decrease of inter-aggregate space, and a significant creep deformation is induced by the progressive closure of intra-aggregate pores in the bentonite clay matrix (De Jong and Verruijt, 1965; Navarro and Alonso, 2001; Le, *et al.*, 2012; Fatahi *et al.*, 2013; Choo and Borja, 2015; Sánchez *et al.*, 2016; Choo *et al.*, 2016). Analyzing the time-depend compressibility of the sand-bentonite mixtures is important for preventing the migration of contaminants from waste disposal vault.

The deformation behavior of gap-graded binary mixtures was documented by many researchers (E.g., Yin 1999a; Reil *et al.*, 2002; Monkul and Ozden, 2007; Watabe *et al.*, 2011; Polidori 2007 and 2015; Fatahi, and Khabbaz, 2013; Elkady *et al.*, 2015; Chu *et al.*, 2017; Sun *et al.*, 2017). Most of the previous work is based on the laboratory element tests and the corresponding analysis is empirical or semi-empirical (e.g., Yin 1999a; Polidori 2015; Sun *et al.*, 2017). It revealed that there was a 'transition clay content', beyond which the overall

compressibility was controlled by the sand skeleton (Monkul and Ozden, 2007, Sun *et al.*, 2017). The intergranular structure evolution was incorporated into a compression model (Shi and Yin, 2017) using homogenization approach.

The time dependent compression behavior of sand-bentonite mixtures is investigated in this paper, both experimentally and theoretically. Since the initial water content affects the compressibility of clays (Hong *et al.*, 2010; Shi and Herle, 2015; Cerato and Lutenegger., 2015; Zeng *et al.*, 2015 and 2016; Zhou *et al.*, 2016; Horpibulsuk *et al.*, 2016; Bian *et al.*, 2016; Bian *et al.*, 2017; Shi and Yin, 2017), both the influence of sand fraction and the initial water content of the bentonite matrix is incorporated in the subsequent analysis.

Definition of state dependent variables

Sand-bentonite mixtures consist of sand particles and the bentonite clay matrix within the inter-granular space. If it is assumed that the sand inclusions do not have any water holding capacity (Mitchell, 1993), the binary mixture is composed of silts, clay particles, fluids and sand particles. The silts and clay particles are the solid phases (the volume is denoted as V_{sb}) in the bentonite matrix, and the overall compressibility is induced by the dissipation of fluid phase (denoted as V_{fb} in representative elementary volume). The volume of sand inclusions is represented as V_{ss}, thus the corresponding volume fraction ϕ_s is given as

$$\phi_s = \frac{V_{ss}}{V_{fb} + V_{sb} + V_{ss}} \tag{1}$$

Since the sand inclusions are assumed to be incompressible, the volume fraction of sand inclusions increases with the decrease of the volume of clay matrix. Therefore, ϕ_s is a state dependent variable, which can be expressed as a function of the overall and local void ratios:

$$\phi_s = \left(\frac{V_{fb}}{V_{sb}} - \frac{V_{fb}}{V_{sb} + V_{ss}} \right) \left(\frac{V_{sb} + V_{ss}}{V_{fb} + V_{sb} + V_{ss}} \right) \frac{V_{sb}}{V_{fb}} = \frac{e_b - e}{(1+e)e_b} \tag{2}$$

With $e_b = V_{fb} / V_{sb}$ denoting the local void ratio of the bentonite clay matrix, and $e = V_{fb} / (V_{sb} + V_{ss})$ denoting the overall void ratio of the sand-bentonite mixture, respectively.

The stress (strain) distribution is nonuniform due to the difference in stiffness between the sand inclusions and soft bentonite matrix. (Weng and Tandon, 1988; Shi and Herle, 2017; Shi and Yin, 2017; Shi *et al.*, 2017). To this end, the stress and strain variables are defined as volume average values. Within mixture theory, the overall stress σ' (or strain ε) can be expressed in terms of the local values:

$$\sigma' = (1-\phi_s)\sigma'_b + \phi_s \sigma'_s; \quad \varepsilon = (1-\phi_s)\varepsilon_b \tag{3}$$

where σ'_b (or σ'_s) and ε_b are the volume average stress and strain in the bentonite matrix (or sand inclusions), respectively. Note that the overall strain of mixtures depends on the local strain of the clay matrix due to the incompressible sand inclusions.

The void ratios in Eq. (2) can be easily computed based on the initial overall (local) void ratio and the current overall (local) strain of the mixture. The above state variables can be well defined using a limited number of inclusions within representative volume element (RVE) concept (González *et al.*, 2004; Shi and Herle, 2017; Shi and Yin, 2017) on this type of binary mixtures.

Time dependent deformation of sand-bentonite mixtures

Materials and test program

The materials used for the binary mixtures are a silica sand material (coarse inclusions) and a bentonite (clay matrix). Most of the sand particles have a sub-angular shape with a particle size ranging from 1.0 mm to 2.0 mm. The maximum and minimum void ratios of the sand material are 0.89 and 0.55, respectively. The above two limit void ratios are important for

evaluating the evolution of the sand skeleton during the compression of sand-bentonite mixtures. The bentonite has a liquid limit of 524% and a plastic limit of 64%. The above basic physical properties are measured according to BS1377 (British Standards Institution, 1991).

As stated above, the initial water content affects the compressibility of clays during primary consolidation. However, the effect of initial water content on the creep behavior was rarely reported. To investigate this effect, water was added to the dry bentonite to get two different initial water contents of the bentonite slurry, a higher value of 885% (1.69 w_L) and a lower one of 744% (1.42 w_L). After that, silica sand particles and bentonite slurry were mixed homogeneously with various sand mass fractions υ (υ is defined as the ratio of the dry mass of sand inclusions to the overall dry mass of the sand-bentonite mixture. Four different mass fractions for the slurry with a higher initial water content, 0%, 50%, 65%, and 75%; three different mass fractions for the one with a lower initial water content, 0%, 65%, and 75%). Then, the samples were kept in an airtight container for 48 hours to make them fully saturated. Since the initial water content is relatively high, the sand mass fraction adopted in this paper is higher than those in previous literature (E.g., Yin, 1999a; Monkul and Ozden, 2007; Zhou and Xu, 2015; Chu *et al.*, 2017; Shi and Yin, 2017). In this case, the volume of the bentonite matrix is high enough to fill the inter-granular space.

The sample has a height of 19 mm and a diameter of 50 mm. A small initial stress of ca. 1.7 kPa was applied to the sample, which prevents soil squeezing from the gap between the loading cap and the consolidation ring. Subsequent consolidation stresses were 2.5, 5.0, 10, 25, 50, 100, 200, 400 (800) kPa. The time duration at stress levels beyond 10 kPa is more than 5000 mins. To investigate the long-term creep behavior of the sand-bentonite mixtures, the samples were loaded for 11295 mins at a stress level of 100 kPa.

Time dependent compression behavior

In the sequel, the logarithmic strain is adopted for the creep analysis due to high

compressibility of the samples (ε=ln(h_0/h), with h_0 and h representing the initial and current heights of mixture samples, respectively). The time dependent overall strain of the sand-bentonite mixtures at various stress levels is shown in Fig. 1. The overall compression can be divided into the primary consolidation and creep deformation. The end of primary consolidation (EOP) point can be determined using Casagrande method. It reveals that the time duration responsible for the primary consolidation is less than 1 day (1440 mins) at stress levels beyond 10 kPa.

A reference time line should be determined for subsequent creep analysis. It corresponds to either the end of primary consolidation or 24 hours in the laboratory testing (Yin, 2015; Yin and Feng, 2016). Since the end of 'primary consolidation' is less than 24 hours, the latter one (24 hours) is adopted for the reference time line. The reference time line for sand-bentonite mixtures with different initial water contents and different sand fractions are shown in Fig. 2 (in terms of the overall strain and the overall effective stress). The overall compressibility decreases with increasing sand fraction due to the incompressible sand inclusions. Additionally, the reference time line is not unique, which varies with the initial water content of the bentonite matrix.

The current overall void ratio of the samples is computed from its initial value and the corresponding logarithmic strain:

$$e = (1+e_0)\exp(-\varepsilon) - 1 \tag{4}$$

The results of oedometer tests in terms of overall effective stress and overall specific volume ($v = 1 + e$) are shown in Fig. 3 (semi-logarithmic scale). It is seen that the compression data with various initial water contents and various sand fractions can be approximated by a linear relationship in semi-logarithmic plot.

$$v_{24} = N_{24} - \lambda_{24}\ln(\sigma'/\sigma_r) \tag{5a}$$

$$v_{b,24} = N_{b,24} - \lambda_{b,24}\ln(\sigma'_b/\sigma_r) \tag{5b}$$

where $N_{b,24}$ and $\lambda_{b,24}$ are intrinsic compression parameters of bentonite matrix responsible for the reference time line, N_{24} and λ_{24} are the corresponding overall values of sand-bentonite mixtures, σ_r =1 kPa is a reference stress.

The sand-bentonite mixtures investigated in this study are binary mixtures, i.e., the inter-granular space is fully filled with bentonite slurry. Considering that the sand particles are incompressible, one gets the relationship between the local void ratio of the bentonite matrix and the overall void ratio of the mixture:

$$e_b = \frac{(1-\upsilon)\rho_s + \upsilon\rho_b}{(1-\upsilon)\rho_s} e \tag{6}$$

where ρ_s and ρ_b are the particle density of the sand inclusions (2.69 g/cm^3) and bentonite matrix (2.70 g/cm^3), respectively.

The specific volume is usually incorporated into constitutive models in classical soil mechanics, e.g., Cam-clay model. Therefore, we use the specific volume as the state variable, which can be easily extended to a general case. The overall creep parameter of sand-bentonite mixtures is defined as the slope of specific volume versus the logarithm of creep time.

$$\psi = -\frac{\delta v}{\delta(\ln t)} = -\frac{\delta e}{\delta(\ln t)} \tag{7}$$

A linear relationship in terms of the specific volume versus logarithm of creep time is given as

$$v = v_0 - \psi \ln\left(\frac{t_0 + t_e}{t_0}\right) \tag{8}$$

where t_0 =1440 mins, v_0 is the corresponding overall specific volume on the reference time line, t_e is the equivalent creep time beyond 1440 mins at a given stress level. After Yin (1999b), Feng *et al.* (2017), and Hu *et al.* (2014), soils usually exhibit nonlinear creep behavior: the creep parameter decreases with creep time. To investigate the effect of time duration on the creep

parameter, the sand-bentonite mixture samples were loaded at 100 kPa for more than 10000 mins. The long-term creep data are shown in Fig. 4. It is seen that the linear relationship given in Eq. (8) is well consistent with the test data within the duration time (11295 mins) and test stress level (effective vertical stress =100 kPa). In the sequel, Eq. (8) would be adopted for the creep analysis of the sand-bentonite mixtures. Note that the relationship between the specific volume and logarithm of creep time may change with the choice of t_0. If a lower value of t_0 is adopted, the specific volume may change nonlinearly with the logarithm of creep time (Yin, 1999b).

Since the sand particles are incompressible, the overall creep deformation is induced by the creep of bentonite matrix. The local creep parameter of the bentonite matrix is introduced:

$$\psi_b = -\frac{\delta v_b}{\delta(\ln t)} = -\frac{\delta e_b}{\delta(\ln t)} \tag{9}$$

Combining Eqs. (6), (7) and (9), the following equation can be obtained:

$$\psi = \frac{(1-\upsilon)\rho_s}{(1-\upsilon)\rho_s + \upsilon\rho_b}\psi_b \tag{10}$$

Discussion on the creep parameters

Overall creep behavior

The overall creep deformation of sand-bentonite mixtures depends on the local deformation of the bentonite matrix (Eq. (10)), therefore, the intrinsic creep behavior of bentonite matrix is investigated as a reference for assessing the overall behavior. The (overall) creep parameter in the following analysis is calibrated using Eq. (8) and the data points presented in Fig. 1. The test results of the pure bentonite with two different initial water contents are shown in Fig. 5 in terms of the creep parameter ψ_b^* and the effective vertical stress. It is seen that the creep parameter shows a nonlinear decrease with increasing effective vertical stress. Additionally, the creep parameter of the sample with a lower initial water content (1.42 w_L) is approximately

close to that of the one with a higher initial water content (1.69 w_L) at a given stress level. This indicates that the influence of initial water content on the creep formation is negligible for the bentonite used in this study. Therefore, the creep behavior of bentonite matrix is noted as the 'intrinsic' one. A double logarithmic function can well reproduce the relationship between the intrinsic creep parameter and the effective vertical stress:

$$\psi_b^* = \alpha_b^* \left(\frac{\sigma'}{\sigma_r} \right)^{\beta_b^*} \tag{11}$$

To show the effect of sand mass fraction on the creep behavior of the sand-bentonite mixtures, the results of the mixtures with a given initial water content are shown in Fig. 6. It can be seen that the data points of the overall creep parameter are located below the intrinsic line of the pure bentonite. The overall creep parameter decreases with an increase of the sand mass fraction due to the increasing volume fraction of incompressible sand inclusions. For a given sand mass fraction, the influence of initial water content of the clay matrix on the overall creep parameter is shown in Fig. 7. Analogous to the pure bentonite in Fig. 5, the data points with different initial water contents are approximately close at a given stress level, hence, the influence of the initial water content of the bentonite matrix can be neglected in geotechnical point of view.

Local creep behavior

The local creep parameter of the bentonite matrix is computed from Eq. (10), the data are summarized in Fig. 8 in terms of the local creep parameter and the overall effective mean stress. It is seen that the data points are almost consistent with the intrinsic line of the pure bentonite matrix for a lower sand mass fraction (υ=50%). The corresponding volume fraction of the sand inclusions varies from 0.05 (5kPa) to 0.20 (400 kPa). This is due to the fact that the stress distribution in binary mixtures is relatively uniform for such a low volume fraction of sand inclusions (Shi and Herle, 2017, Shi and Yin, 2017). For clarifying the stress distribution in the sand-bentonite mixtures, the local strain (deformation related to the primary consolidation) of

the bentonite matrix is calculated (Eq. (3)) and is presented in Fig. 9 in terms of the local strain and the overall effective stress. It is seen from Fig. 9(a) that the test data of the mixtures with a sand mass fraction of 50% is approximately close to those of the pure bentonite soil. It reveals that the local stress in the bentonite matrix is close to the overall value of the mixture sample. Therefore, the creep deformation of the bentonite matrix in sand-bentonite mixtures is almost the same as the one of the pure bentonite at a given stress level (Fig. 8).

Analogous to the overall creep parameter, the local creep parameter of the bentonite matrix decreases with the increase of the sand mass fraction. Correspondingly, the data points of local permeability move downwards and are located below the intrinsic line of pure bentonite. It can be seen from Fig. 9 that the stress-strain curve tends to move downwards with increasing sand fraction, indicating that the stress distribution becomes more nonuniform and the stress in the sand inclusions is higher than that in the bentonite matrix. Moreover, the inhomogeneity of the bentonite matrix increases with increasing sand fraction, and the stress and strain distribution in the bentonite matrix is becoming more nonuniform. This can be explained by Fig. 10, the clay between adjacent sand inclusions are being densified, and clay bridges form. The stress and strain in the clay-bridge zones is higher than the corresponding average values in the bentonite matrix. This concept was adopted by many researchers for clarifying different mechanisms of binary sand-clay mixtures (E.g., Jafari and Shafiee, 2004; Fei, 2016; Deng *et al.*, 2017; Shi and Yin, 2017). However, the so-called ‘clay-bridge’ is not stable, which may break down and be replaced by a new one with increasing stress level.

A creep model using homogenization approach

Structure variables and creep model

The sand-bentonite mixtures consist of rigid sand inclusions and very soft bentonite clay

matrix. As stated by Hashin (1983) and Tu *et al.* (2005), the overall stiffness of these mixtures increases with the increase of sand fraction, however, it can approach only several times of the local stiffness of the matrix stiffness. Based on series of oedometer tests on sand-marine clay mixtures, Shi and Yin proposed a double logarithmic relationship between the overall tangent stiffness of the mixtures and local tangent stiffness of the clay matrix (Shi and Yin, 2017):

$$\ln\left(\frac{E_{24}}{\sigma_r}\right)=\chi(1-\phi_s)\ln\left(\frac{E_{b,24}}{\sigma_r}\right) \tag{12}$$

where $E_{b,24}$ and E_{24} are the local tangent stiffness of the bentonite clay matrix and the overall value of the mixtures, respectively. χ represents the inter-granular structure evolution of the sand inclusions. As a structure variable, it is approximately close to 1 in case of a negligible volume fraction of the sand inclusions. Additionally, when the volume fraction of the sand inclusions reaches its maximum value (corresponding to the minimum void ratio of the sand skeleton), any further loading would be overtaken by the sand skeleton alone. Consequently, the structure variable becomes infinite. The structure variable increases with the volume fraction of sand inclusions, which can be expressed as

$$\chi=\left(\frac{\vartheta}{\vartheta-\phi_s}\right)^{\xi} \tag{13}$$

where ϑ is upper limit of the volume fraction of sand inclusions corresponding to the minimum void ratio of the sand skeleton $e_{\min}$: $\vartheta=1/(1+e_{\min})$. ξ is a constant model parameter which controls the sensitivity of the structure variable χ on the sand volume fraction ϕ_s. Normally, ξ falls in between 0.5 and 1.0. For the sand material used in this study, the minimum void ratio of the sand skeleton e_{min}=0.55, the model parameter ξ can be calibrated by using Eq. (13) and the test data of sand-bentonite mixtures, see Fig.11. ξ=0.8 can well fit the data points in Fig. 11 regardless of the sand mass fraction and initial water content of the bentonite matrix.

As stated above, the presence of clay-bridges between adjacent sand inclusions prevents

282 further creep deformation, leading to a decrease of local creep parameter of the bentonite matrix.
283 An equivalent local creep parameter $\hat{\psi}_b$ is introduced for assessing the creep deformation of
284 the mixtures. It is defined as

285 $$\hat{\psi}_b = \alpha_b^* \left(\frac{\sigma'}{\sigma_r} \right)^{\beta_b^*} \tag{14}$$

286 With σ' denoting the overall effective vertical stress in sand-bentonite mixtures. Eq. (14)
287 means that the equivalent local creep parameter equals the creep parameter of the pure bentonite
288 at the same effective vertical stress (It is assumed that the local stress in the bentonite matrix
289 equals the overall value in the matrix). Another structure variable $\hat{\chi}$ is defined as the ratio of
290 the equivalent local creep parameter to the actual value calculated from Eq. (10).

291 $$\hat{\chi} = \frac{\hat{\psi}_b}{\psi_b} \tag{15}$$

292 Note that, χ and $\hat{\chi}$ are structure variables, which are associated with the state of the sand-
293 clay mixtures. They are different from ξ which is a constant structure parameter. The evolution
294 of the structure variable $\hat{\chi}$ with the volume fraction of sand inclusions is shown in Fig. 12. The
295 theoretical curve of the structure variable χ (refer to Eq. (13)) is also plotted in this figure. It
296 is seen that the structure variable $\hat{\chi}$ increases with the volume fraction of sand inclusions, and
297 the data points are well consistent with the structure variable χ. Therefore, the local creep
298 parameter can be expressed as

299 $$\psi_b = \frac{\hat{\psi}_b}{\chi} = \alpha_b^* \left(\frac{\sigma'}{\sigma_r} \right)^{\beta_b^*} \left(\frac{\vartheta}{\vartheta - \phi_s} \right)^{-\xi} \tag{16}$$

300 Substituting Eq. (16) into Eq. (10), the following creep model is obtained:

301 $$\psi = \frac{(1-\upsilon)\rho_s \alpha_b^*}{(1-\upsilon)\rho_s + \upsilon\rho_b} \left(\frac{\sigma'}{\sigma_r} \right)^{\beta_b^*} \left(\frac{\vartheta}{\vartheta - \phi_s} \right)^{-\xi} \tag{17}$$

Evolution of sand volume fraction

There are two state variables in Eq. (17), the overall effective stress σ' and the volume fraction of the sand inclusions ϕ_s. Since the sand inclusions are incompressible, the volume fraction of the sand inclusions decreases with increasing stress level. Following the model procedure proposed by Shi and Yin (2017), the sand volume fraction at a given stress level can be computed.

The from the compression model of the bentonite Eq. (5b), the tangent stiffness of the bentonite matrix is deduced as

$$E_{b,24} = \frac{\mathrm{d}\sigma'_b}{\mathrm{d}\varepsilon_{b,24}} = -\frac{\mathrm{d}\sigma'_b}{\mathrm{d}(\ln v_{b,24})} = \frac{v_{b,24}\sigma'_b}{\lambda_{b,24}} \tag{18}$$

With $\varepsilon_{b,24}$ denoting the local strain of the bentonite matrix corresponding a loading period of 24 h. Note that the strain used in Eq. (18) are defined as logarithmic strain. Considering the definition of the overall tangent stiffness, substitution of Eq. (18) into Eq. (12) gives

$$E_{24} = \frac{\mathrm{d}\sigma'}{\mathrm{d}\varepsilon_{24}} = \sigma_r \left(\frac{E_{b,24}}{\sigma_r}\right)^{\chi(1-\phi_s)} = \sigma_r \left(\frac{v_{b,24}\sigma'_b}{\lambda_{b,24}\sigma_r}\right)^{\chi(1-\phi_s)} \tag{19}$$

A significant difference in stiffness between the sand inclusions and the bentonite matrix leads to a nonuniform stress distribution in the sand-bentonite mixtures. To consider this effect, an incremental stress ratio is defined as the ratio of the local stress increment (bentonite matrix) to the overall stress increment:

$$\mu_\sigma = \frac{\mathrm{d}\sigma'_b}{\mathrm{d}\sigma'} \tag{20}$$

The stress concentration variable μ_σ can be uniquely defined using the local stiffness and the overall stiffness of the mixtures (Hill, 1963). Combining Eqs (3), (18)-(20) yields

$$\mu_\sigma = \frac{1}{1-\phi_s}\left(\frac{v_{b,24}\sigma'_b}{\lambda_{b,24}\sigma_r}\right)^{1-\chi(1-\phi_s)} \tag{21}$$

For a given overall load increment, the local stress increment can be computed from the stress concentration variable. Then, the local and overall strains can be determined, and the volume fraction of the sand fraction is computed afterwards. The numerical procedures would be given in details in the next section.

Numerical procedures and validation of the model

Remolded yield stress as a reference point for calculation

For reproducing the compression curve of mixture samples, the starting point of Normal Compression Line (e.g., a specified void ratio and corresponding stress state) should be determined. For this purpose, the remolded yield stress for reconstituted soils proposed by Hong (2010) was adopted in this study. It is linked to suction pressure on the surface of soil samples arises during the sample preparation process (Hong *et al.*, 2006; Shi and Herle, 2015). The remolded yield stress decreases with the increase of initial water content of oedometer samples (Hong, 2007; Hong *et al.*, 2010; Shi and Herle, 2015; Shi and Herle, 2016). It is assumed that no deformation occurs within the remolded yield stress (Hong, 2007). In this case, the remolded yield stress can be estimated by extrapolating the Normal Compression Line to the initial void ratio e_0 of the binary mixtures:

$$\sigma'_y = \exp\left(\frac{N_{24} - 1 - e_0}{\lambda_{24}}\right) \tag{22}$$

Correspondingly, the compression curve of the binary mixtures is characterized by two regimes: the suction preloading regime below the remolded yield stress σ'_y and the post-yield regime beyond σ'_y. The deformation is negligible when the consolidation stress is lower than σ'_y ($e = e_0$). However, the stiffness decreases and the compression data beyond the remolded yield stress can be reproduced by the proposed compression model (Eqs (2), (13), (18)-(21)).

The remolded yield stress of sand-bentonite mixtures in given in Table 1. It corresponds to

the assumption that no deformation occurs within the remolded yield stress. This assumption may lead to an underestimation of the remolded yield stress (Hong *et al*., 2010). However, the remolded yield stress is extremely low, and such a low stress is not of interest in engineering practice. The real remolded yield stress should be slightly higher than that in Table 1. In this case, the soil squeezing could be avoided at a stress level of 1.7 kPa.

Model parameters and calibration

From the model presented above (Eqs (2), (13), (17)-(21)), five parameters need to be calibrated for the creep model: α_b^*, β_b^*, $N_{b,24}$, $\lambda_{b,24}$, ξ. The first four parameters depend on the intrinsic behavior of the pure bentonite, and the last one is related to the structure evolution of sand skeleton in the mixture. The physical meaning and the calibration of the model parameter are summarized as follows: α_b^*, β_b^* are the creep parameters, which are calibrated from the creep data of the pure bentonite; $N_{b,24}$, $\lambda_{b,24}$ are intrinsic compression parameters of the bentonite. They can be calibrated from the compression data of the pure bentonite beyond the remolded yield stress. The effect of the structure evolution of sand skeleton in the binary mixtures is incorporated into the model by introducing the structure parameter ξ.

Two oedometer tests need to be done for calibrating the above parameters: one test on the pure bentonite and the other on a sand-bentonite mixture with a predefined sand mass fraction. Note that the time duration at each surcharge loading should be long enough for the analysis of creep behavior. The local creep parameter of the pure bentonite is determined using Eq. (9), then, the intrinsic creep parameters α_b^*, β_b^* are calibrated in terms of the relationship between the local creep parameter and the effective vertical stress, as shown in Fig. 5. The intrinsic compression parameters $N_{b,24}$, $\lambda_{b,24}$ are calibrated according to the reference time line of the bentonite clay in semi-logarithmic $v-\ln\sigma'$ plot, as shown in Fig. 3. Note that the reference time line of bentonite is not unique, which depends on the initial water content. Hence, the

intrinsic compression parameters $N_{b,24}$, $\lambda_{b,24}$ for the two series of tests (one with a lower initial water content of the bentonite matrix and the other with a higher value) are different. The structure parameter ξ is calibrated based on the data of a sand-bentonite mixture, by trial and error method through the relationship between the structure variable χ and the volume fraction of the sand inclusions, as shown in Fig. 11. It is expected that the structure parameter ξ is influenced by the shape of sand inclusions and the particle size distribution of the sand material. The calibrated model parameters for the tested materials are given in Table 1.

Numerical procedures

The full model consists of two parts: calculation of the volume fraction of the sand inclusions and computing the creep parameter afterwards. The computation procedures of the proposed are given as follows:

(1) Estimating the remolded yield stress of the mixtures σ'_y. A reference point (σ'=σ'_y, e=e_0) is adopted as the initial state of the mixture.

(2) It is assumed that the stress distribution in the mixture is uniform at the reference point (σ'_y, e_0), i.e., $\sigma'_b = \sigma'_s = \sigma'$. The work done by previous researchers reveals that the undrained shear stress of remolded sand-clay mixtures is approximately close to that of the clay matrix (e.g., Stone and Kyambadde, 2012; Cabalar and Mustafa, 2015). This reveals that the stress in the sand-clay matrix is almost uniform at the fully remolded state.

(3) For a given overall effective stress increment at the *k*th incremental step $(\mathrm{d}\sigma')^k$, the current local effective stress increment of the bentonite matrix is $(\mathrm{d}\sigma'_b)^k = \mu_\sigma^{k-1}(d\sigma')^k$ (μ_σ^{k-1} is the incremental stress ratio at the *k*th incremental step).

(4) The overall strain and stress at the last incremental step are denoted as $(\sigma')^{k-1}$ and $(\varepsilon_{24})^{k-1}$, respectively. The overall and local stresses are updated as: $(\sigma')^k = (\sigma')^{k-1} + (\mathrm{d}\sigma')^k$;

$(\sigma_b')^k = (\sigma_b')^{k-1} + (\mathrm{d}\sigma_b')^k$.

(5) Compute the overall strain increment $(\mathrm{d}\varepsilon_{24})^k$ and the local strain increment of the bentonite matrix $(\mathrm{d}\varepsilon_{b,24})^k$: $(\mathrm{d}\varepsilon_{24})^k = \dfrac{(\mathrm{d}\sigma')^k}{(E_{24})^{k-1}}$; $(\mathrm{d}\varepsilon_{b,24})^k = \dfrac{(\mathrm{d}\sigma_b')^k}{(E_{b,24})^{k-1}}$. $(E_{24})^{k-1}$ and $(E_{b,24})^{k-1}$ denote the overall and local stiffness at the last incremental step, refer to Eqs (18) and (19).

(6) The overall strain and local strain of bentonite are updated as: $(\varepsilon)^k = (\varepsilon)^{k-1} + (\mathrm{d}\varepsilon)^k$; $(\varepsilon_b)^k = (\varepsilon_b)^{k-1} + (\mathrm{d}\varepsilon_b)^k$. The current void ratios are calculated as

$$(e)^k = (1+e_0)\exp(-\varepsilon)^k - 1;\ (e_b)^k = (1+e_{b0})\exp(-\varepsilon_b)^k - 1 \tag{23}$$

(7) The volume fraction of sand inclusions at the current incremental step (denoted as $(\varphi_s)^k$) is updated using Eqs (2) and (23).

(8) The overall creep parameter at the current incremental step $(\psi)^k$ is calculated according to Eq. (17).

(9) The structure variable at the current step χ^k is computed according to Eq. (13) and the updated volume fraction of sand inclusions. The stress incremental ratio at the current incremental step μ_σ^k is then computed using Eq. (21).

(10) For the next incremental step, repeat Steps (3)-(9).

Validation of the model

Following the numerical procedures listed above, the oedometer data of the sand-bentonite mixtures is reproduced using the model parameters given in Table 1. Fig. 13 shows the simulated compression curves of the mixtures in terms of the specific volume and the overall effective stress. It is seen that the model can well reproduce the compression data with different sand mass fractions and different initial water content of the bentonite matrix. Note that different compression parameters are adopted for the different initial water content of the

bentonite matrix, since the initial water content significantly affects the reference time line of the pure bentonite. The evolution of the volume fraction of sand inclusions is shown in Fig. 14, indicating an excellent consistence between the experimental data point and the model prediction. Correspondingly, the structure parameter χ is calculated at a given stress level, which is shown in Fig.15 together with the experimental data. It is seen that some differences arise between the model prediction and test data. This may be induced by the assumption of a uniform stress distribution at the remolded yield stress. However, the differences vanish after approaching an overall effective stress of 25 kPa. Finally, the local creep parameter is computed using Eq. (16), and model prediction is shown in Fig. 16. The overall creep parameter is calculated and is presented in Fig. 17 in terms of the overall creep parameter and the overall effective stress. Comparison between the model prediction and experimental data reveals a satisfactory performance of the proposed model.

Conclusions

The sand-bentonite mixtures show a considerable creep deformation. To analyze of the creep behavior, a series of oedometer tests was performed on the binary mixtures, and an analytical model was proposed for reproducing the laboratory data. The main conclusions of this study are summarized as follows:

(1) Oedometer tests on sand-bentonite mixtures reveal that the reference time line (corresponding to 24h of consolidation) is significantly affected by both the initial water content and the sand mass fraction. However, the influence of initial water content of the bentonite matrix on the overall creep behavior seems to be neglected.

(2) The local creep parameter with a sand mass fraction of 50% is approximately close to that of the pure bentonite due to a relatively low volume fraction of sand inclusions. However, the local creep parameter of the bentonite matrix decreases with the further increase of

sand mass fraction (65% and 75%). This phenomenon is accompanied by increasing inhomogeneity of the binary mixtures, and it can be explained by a formation of clay-bridges between adjacent sand inclusions.

(3) An equivalent local creep parameter is introduced for assessing the creep deformation of the mixtures, and a new structure variable $\hat{\chi}$ is defined as the ratio of the equivalent local creep parameter to the actual value. Analysis on the laboratory data shows that the structure variable $\hat{\chi}$ can be approximated by the one for the inter-granular structure evolution χ.

(4) A model is proposed for the creep behavior of sand-bentonite mixtures. The overall creep parameter depends on the volume fraction of sand and the structure parameter controlling the inter-granular structure evolution of sand inclusions. The evolution of volume fraction is computed based on the model for reference time line of the binary mixtures.

(5) The proposed creep model has five parameters, four of them represent the intrinsic behavior of the pure bentonite, and a structure parameter incorporating the inter-granular structure effects. The parameters can be easily calibrated based on two conventional oedometer tests. Comparison between the model prediction and test data reveals that the model performance is satisfactory for reproducing the creep behavior of the sand-bentonite mixtures.

List of symbols

e	Overall void ratio of sand-bentonite mixtures
e_0	Initial overall void ratio of sand-bentonite mixtures
e_b	Void ratio of bentonite matrix in sand-bentonite mixtures
$e_{\min}$	The minimum void ratio of sand skeleton
E_{24}	Tangent stiffness corresponding to the reference time line of sand-bentonite mixtures
$E_{b,24}$	Tangent stiffness corresponding to the reference time line of bentonite matrix
h_0	Initial height of the test samples (sand-bentonite mixtures)
h	Height of the test samples during loading process (sand-bentonite mixtures)
N_b	Overall specific volume on reference time lines of mixtures at a stress of 1.0 kPa
$N_{b,24}$	Specific volume on reference time lines of bentonite at a stress of 1.0 kPa
t_e	Equivalent creep time beyond 1440 mins at a given stress level
v	Overall specific volume of sand-bentonite mixtures
v_0	Initial overall specific volume of sand-bentonite mixtures
v_{24}	Initial overall specific volume on reference time lines
v_b	Specific volume of bentonite matrix
$v_{b,24}$	Initial specific volume of bentonite matrix on reference time lines
V_{ss}	Volume of sand inclusions
V_{sb}	Volume of solid phase in bentonite matrix
V_{fb}	Volume of fluid phase in bentonite matrix
w_L	Liquid limit of sand-bentonite mixtures

α_b^* (β_b^*) Intrinsic creep parameters of the pure bentonite

ε_{24} Strain corresponding to the reference time line of sand-bentonite mixtures

$\varepsilon_{b,24}$ Strain corresponding to the reference time line of bentonite

λ_{24} Slope of the reference time line of sand-bentonite mixtures

$\lambda_{b,24}$ Slope of the reference time line of bentonite matrix

μ_σ Stress incremental ratio

ξ Constant model parameter controlling the sensitivity of the structure parameter on the sand volume fraction

ϑ Upper limit of the volume fraction of sand inclusions

ρ_b Density of soil particles of bentonite matrix

ρ_s Density of soil particles of sand inclusions

σ' Overall stress in sand-bentonite mixtures

σ'_b Stress in bentonite matrix in sand-bentonite mixtures

σ_r A unit reference stress of 1.0 kPa

σ'_s Stress in sand inclusions in sand-bentonite mixtures

σ'_y Remolded yield stress of sand-bentonite mixtures

υ Dry mass fraction of sand inclusions in sand-bentonite mixtures

ϕ_s Volume fraction of sand inclusions

χ Structure variable associated with the inter-granular structure evolution of the sand inclusions

$\hat{\chi}$ Structure variable defined as the ratio of the equivalent local creep parameter to the actual value

ψ Overall creep parameter of sand-bentonite mixtures

510 ψ_b Local creep parameter of bentonite matrix in sand-bentonite mixtures

511 ψ_b^* Creep parameter of pure bentonite

512 $\hat{\psi}_b$ Equivalent local creep parameter of bentonite matrix

513

514

515

516

517

518

519

520

521

522

523

524

525

526

527

528

529

530

531

532

533

534

Acknowledgements

The work in this paper is supported by a National State Key Project "973" grant (Grant No.: 2014CB047000) (sub-project No. 2014CB047001) from Ministry of Science and Technology of the People's Republic of China, a CRF project (Grant No.: PolyU12/CRF/13E), two GRF projects (PolyU 152196/14E; PolyU 152796/16E) from Research Grants Council (RGC) of Hong Kong Special Administrative Region Government of China. The authors also acknowledge the financial supports from Research Institute for Sustainable Urban Development of The Hong Kong Polytechnic University and grants (1-ZVCR, 1-ZVEH, 4-BCAU, 4-BCAW, 5-ZDAF, G-YN97) from The Hong Kong Polytechnic University.

References

Bian, X., Cao, Y. P., Wang, Z. F., Ding, G. Q., & Lei, G. H. (2017). Effect of super-absorbent polymer on the undrained shear behavior of cemented dredged clay with high water content. *Journal of Materials in Civil Engineering*, 29(7).

Bian, X., Wang, Z. F., Ding, G. Q., & Cao, Y. P. (2016). Compressibility of cemented dredged clay at high water content with super-absorbent polymer. *Engineering Geology*, 208, 198-205.

British Standards Institution (1991). Methods of test for soils for civil engineering purposes, *BS 1377*. BSI, Milton Keynes.

Cabalar, A. F., & Mustafa, W. S. (2015). Fall cone tests on clay-sand mixtures. *Engineering Geology*, 192, 154-165.

Choo, J., & Borja, R. I. (2015). Stabilized mixed finite elements for deformable porous media with double porosity. *Computer Methods in Applied Mechanics and Engineering*, 293, 131-154.

Choo, J., White, J. A., & Borja, R. I. (2016). Hydromechanical modeling of unsaturated flow in double porosity media. *International Journal of Geomechanics*, 16(6).

Chu, C., Wu, Z., Deng, Y., Chen, Y., & Wang, Q. (2017). Intrinsic Compression Behavior of Remolded Sand-Clay Mixture. *Canadian Geotechnical Journal*.

De Jong G. J., Verruijt A. (1965). Primary and secondary consolidation of a spherical clay sample. In: *Proceeding of the 6th international conference soil mechanic and foundation engineering*, Montreal, 254-258.

Delage, P., Marcial, D., Cui, Y. J., & Ruiz, X. (2006). Ageing effects in a compacted bentonite: a microstructure approach. *Géotechnique*, 56(5), 291-304.

Deng, Y., Wu, Z., Cui, Y., Liu, S., & Wang, Q. (2017). Sand fraction effect on hydro-mechanical behavior of sand-clay mixture. *Applied Clay Science*, 135, 355-361.

585 Elkady, T. Y., Shaker, A. A., & Dhowain, A. W. (2015). Shear strengths and volume changes
586 of sand-attapulgite clay mixtures. *Bulletin of Engineering Geology and the Environment*,
587 74(2), 595-609.
588 Fatahi, B., & Khabbaz, H. (2013). Influence of fly ash and quicklime addition on behaviour of
589 municipal solid wastes. *Journal of soils and sediments*, 13(7), 1201-1212.
590 Fatahi, B., Le, T. M., Le, M. Q., & Khabbaz, H. (2013). Soil creep effects on ground lateral
591 deformation and pore water pressure under embankments. *Geomechanics and*
592 *Geoengineering*, 8(2), 107-124.
593 Feng, W. Q., Lalit, B., Yin, Z. Y., & Yin, J. H. (2017). Long-term Non-linear creep and swelling
594 behavior of Hong Kong marine deposits in oedometer condition. *Computers and Geotechnics*,
595 84, 1-15.
596 González, C., Segurado, J., & LLorca, J. (2004). Numerical simulation of elasto-plastic
597 deformation of composites: evolution of stress microfields and implications for
598 homogenization models. *Journal of the Mechanics and Physics of Solids*, 52(7), 1573-1593.
599 Graham, J., Oswell, J. M., & Gray, M. N. (1992). The effective stress concept in saturated sand-
600 clay buffer. *Canadian Geotechnical Journal*, 29(6), 1033-1043.
601 Hashin, Z. (1983). Analysis of composite materials. *Journal of Applied Mechanics*, 50(2), 481-
602 505.
603 Hong, Z. S. (2007). Void Ratio-Suction Behavior of Remolded Ariake Clays. *Geotechnical*
604 *Testing Journal*, 30(3), 234-239.
605 Hong, Z. S., Tateishi, Y. and Han, J. (2006). Experimental study of macro and micro-behavior
606 of natural diatomite. *Journal of Geotechnical and Geoenvironmental Engineering, ASCE*.
607 132(5): 603-610.
608 Hong, Z. S., Yin, J., & Cui, Y. J. (2010). Compression behavior of reconstituted soils at high
609 initial water contents. *Géotechnique*, 60(9), 691-700.

610 Horpibulsuk, S., Liu, M. D., Zhuang, Z., & Hong, Z. S. (2016). Complete compression curves
611 of reconstituted clays. *International Journal of Geomechanics*, 16(6).
612 Hu Y.Y., Zhou W.H. and Cai Y. (2014). Large-strain elastic visco-plastic consolidation analysis
613 of very soft clay layers with vertical drains under preloading. *Canadian Geotechnical*
614 *Journal*. 51(2), 144-157.
615 Le, T. M., Fatahi, B., & Khabbaz, H. (2012). Viscous behaviour of soft clay and inducing
616 factors. *Geotechnical and Geological Engineering*, 30(5), 1069-1083.
617 Liu, M. D., Zhuang, Z., & Horpibulsuk, S. (2013). Estimation of the compression behavior of
618 reconstituted clays. *Engineering Geology*, 167, 84-94.
619 Mitchell, J. K. 1993, Fundamentals of Soil Behavior, *John Wiley and Sons*, Inc., New York.
620 Monkul, M. M., & Ozden, G. (2007). Compressional behavior of clayey sand and transition
621 fines content. *Engineering Geology*, 89(3), 195-205.
622 Navarro, V., & Alonso Pérez de Agreda, E. (2001). Secondary compression of clays as a local
623 dehydration process. *Géotechnique*, 51(10), 859-869
624 Nowamooz, H. (2014). Effective stress concept on multi-scale swelling soils. *Applied Clay*
625 *Science*, 101, 205-214.
626 Pal, S. K., & Ghosh, A. (2013). Volume change behavior of fly ash-montmorillonite clay
627 mixtures. *International Journal of Geomechanics*, 14(1), 59-68.
628 Peters, J. F., & Berney IV, E. S. (2009). Percolation threshold of sand-clay binary mixtures.
629 *Journal of Geotechnical and Geoenvironmental Engineering*, 136(2), 310-318.
630 Polidori, E. (2007). Relationship between the Atterberg limits and clay content. *Soils and*
631 *Foundations*, 47, 887-896.
632 Polidori, E. (2015). On the intrinsic compressibility of common clayey soils. *European Journal*
633 *of Environmental and Civil Engineering*, 19(1), 27-47.
634 Revil, A., Grauls, D., & Brévart, O. (2002). Mechanical compaction of sand/clay mixtures.

635 *Journal of Geophysical Research: Solid Earth*, 107(B11).
636 Sánchez, M., Gens, A., Villar, M. V., & Olivella, S. (2016). Fully Coupled Thermo-Hydro-
637 Mechanical Double-Porosity Formulation for Unsaturated Soils. *International Journal of*
638 *Geomechanics*, 16(6).
639 Shi, X. S., & Herle, I. (2015). Compression and undrained shear strength of remoulded clay
640 mixtures. *Géotechnique Letters*, 5(2), 62-67.
641 Shi, X. S., & Herle, I. (2016). Modeling the compression behavior of remolded clay mixtures.
642 *Computers and Geotechnics*, 80, 215-225.
643 Shi, X. S. and Herle, I. (2017). Numerical simulation of lumpy soils using a hypoplastic model.
644 *Acta Geotechnica*, 12(2), 349-363.
645 Shi, X. S., Herle, I., & Muir Wood, D. (2018). A consolidation model for lumpy composite
646 soils in open-pit mining. *Géotechnique*, 68(3), 189-204.
647 Shi X. S., & Yin, J. H. (2017). Experimental and theoretical investigation on remolded sand-
648 marine clay mixtures within homogenization framework. *Computers and Geotechnics*, 90,
649 14-26.
650 Sivapullaiah, P. V., Sridharan, A., & Stalin, V. K. (2000). Hydraulic conductivity of bentonite-
651 sand mixtures. *Canadian Geotechnical Journal*, 37(2), 406-413.
652 Stone, K., & Kyambadde, B. S. (2012). Index and strength properties of clay gravel mixtures.
653 *Proceedings of the ICE-Geotechnical Engineering*, 165(1), 13-21.
654 Sun, W. J., Zong, F. Y., Sun, D. A., Wei, Z. F., Schanz, T., & Fatahi, B. (2017). Swelling
655 prediction of bentonite-sand mixtures in the full range of sand content. *Engineering Geology*,
656 222, 146-155.
657 Thyagaraj, T., Thomas, S. R., & Das, A. P. (2016). Physico-Chemical Effects on Shrinkage
658 Behavior of Compacted Expansive Clay. *International Journal of Geomechanics*, 17(2).
659 Tong, F., & Yin, J. H. (2011). Nonlinear creep and swelling behavior of bentonite mixed with

different sand contents under oedometric condition. *Marine Georesources & Geotechnology*, 29(4), 346-363.

Tu, S. T., Cai, W. Z., Yin, Y., & Ling, X. (2005). Numerical simulation of saturation behavior of physical properties in composites with randomly distributed second-phase. *Journal of composite materials*, 39(7), 617-631.

Vilarrasa, V., Rutqvist, J., Blanco Martin, L., & Birkholzer, J. (2015). Use of a dual-structure constitutive model for predicting the long-term behavior of an expansive clay buffer in a nuclear waste repository. *International Journal of Geomechanics*, 16(6).

Wang, Q., Tang, A. M., Cui, Y. J., Barnichon, J. D., & Ye, W. M. (2013). Investigation of the hydro-mechanical behaviour of compacted bentonite/sand mixture based on the BExM model. *Computers and Geotechnics*, 54, 46-52.

Watabe, Y., Yamada, K., & Saitoh, K. (2011). Hydraulic conductivity and compressibility of mixtures of Nagoya clay with sand or bentonite. *Géotechnique*, 61(3), 211-219.

Weng, G. J., & Tandon, G. P. (1988). A theory of particle-reinforced plasticity. *ASME Journal of Applied Mechanics*, 55(3), 126-135.

Yin, J. H. (1999a). Properties and behavior of Hong Kong marine deposits with different clay contents. *Canadian Geotechnical Journal*, 36(6), 1085-1095.

Yin, J. H. (1999b). Non-linear creep of soils in oedometer tests. *Géotechnique*, 49(5), 699-707.

Yin, J. H. (2015). Fundamental Issues of Elastic Viscoplastic Modeling of the Time-Dependent Stress-Strain Behavior of Geomaterials. *International Journal of Geomechanics*, 15(5).

Yin, J. H., & Feng, W. Q. (2016). A new simplified method and its verification for calculation of consolidation settlement of a clayey soil with creep. *Canadian Geotechnical Journal*, 54(3), 333-347.

Zeng, L. L., Hong, Z. S., & Cui, Y. J. (2015). Determining the virgin compression lines of reconstituted clays at different initial water contents. *Canadian Geotechnical Journal*, 52(9),

1408-1415.

Zeng, L. L., Hong, Z. S., & Gao, Y. F. (2016). Practical estimation of compression behaviour of dredged clays with three physical parameters. *Engineering Geology*.

Zhou, W. H., Garg, A., & Garg, A. (2016). Study of the volumetric water content based on density, suction and initial water content. *Measurement*, 94, 531-537.

Zhou, W. H., & Xu, X. (2014). Unconfined compression strength of unsaturated completely decomposed granite soil with different clay mixing ratios, Geomechanics from Micro to Macro-Soga *et al.*(Eds), Publisher. In *Proceedings of IS-Cambridge 2014*, Cambridge, UK (pp. 1341-1346). Taylor & Francis Group London.

List of Tables

Table 1: Initial state of the oedometer samples and parameters for the proposed model

Samples	w_{b0}	ν	σ'_y	α_b^*	β_b^*	$N_{b,24}$	$\lambda_{b,24}$	ξ
	(%)	(%)	(kPa)	---	---	---	---	---
Series-1	885	0	0.33	1.22	-0.53	22.00	2.75	0.80
Series-1	885	50	0.45	1.22	-0.53	22.00	2.75	0.80
Series-1	885	65	0.39	1.22	-0.53	22.00	2.75	0.80
Series-1	885	75	0.67	1.22	-0.53	22.00	2.75	0.80
Series-2	744	0	0.70	1.22	-0.53	20.23	2.40	0.80
Series-2	744	65	0.72	1.22	-0.53	20.23	2.40	0.80
Series-2	744	75	0.61	1.22	-0.53	20.23	2.40	0.80

Figure1a

Click here to download Figure Figure1a.eps

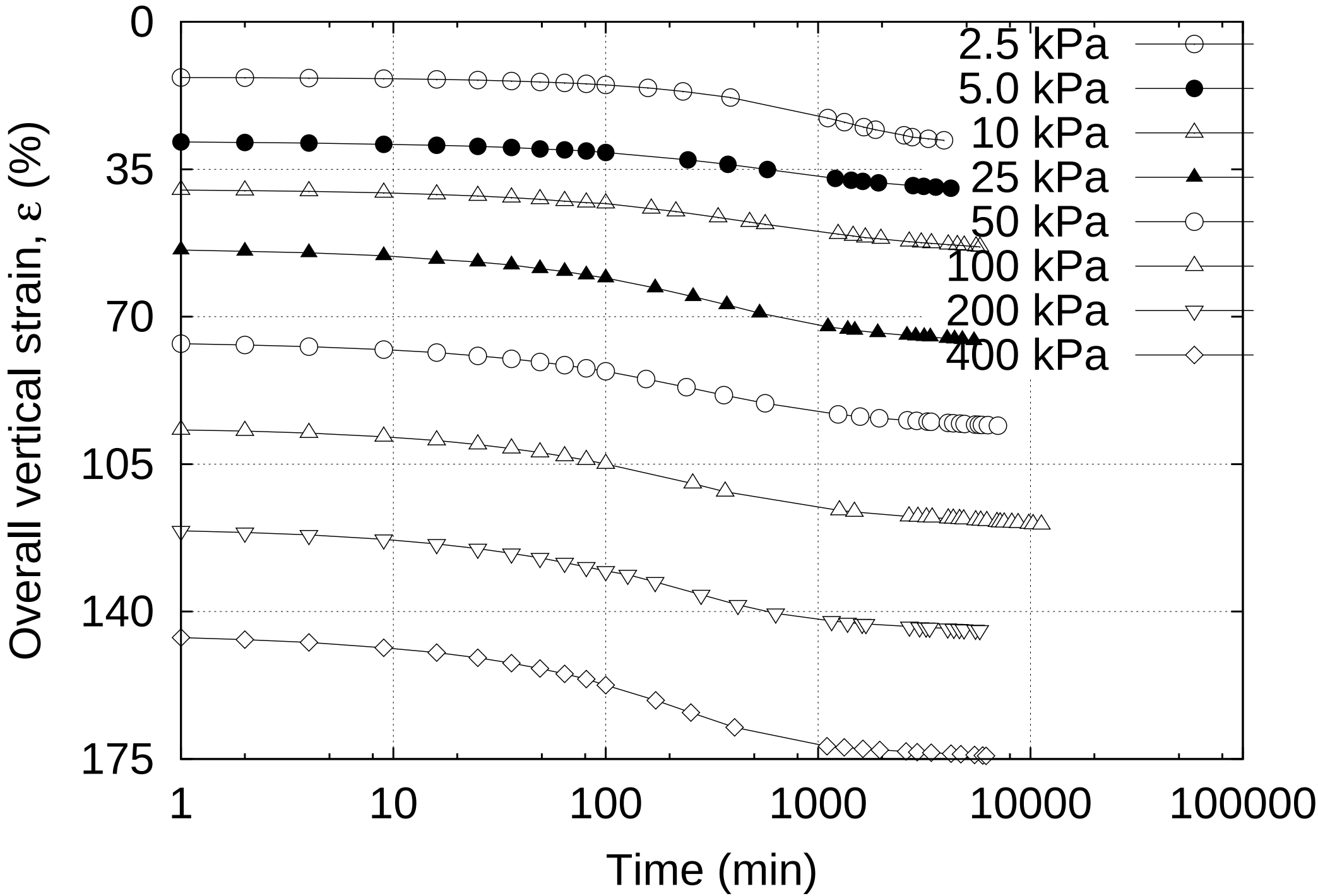

Figure1b

Click here to download Figure Figure1b.eps

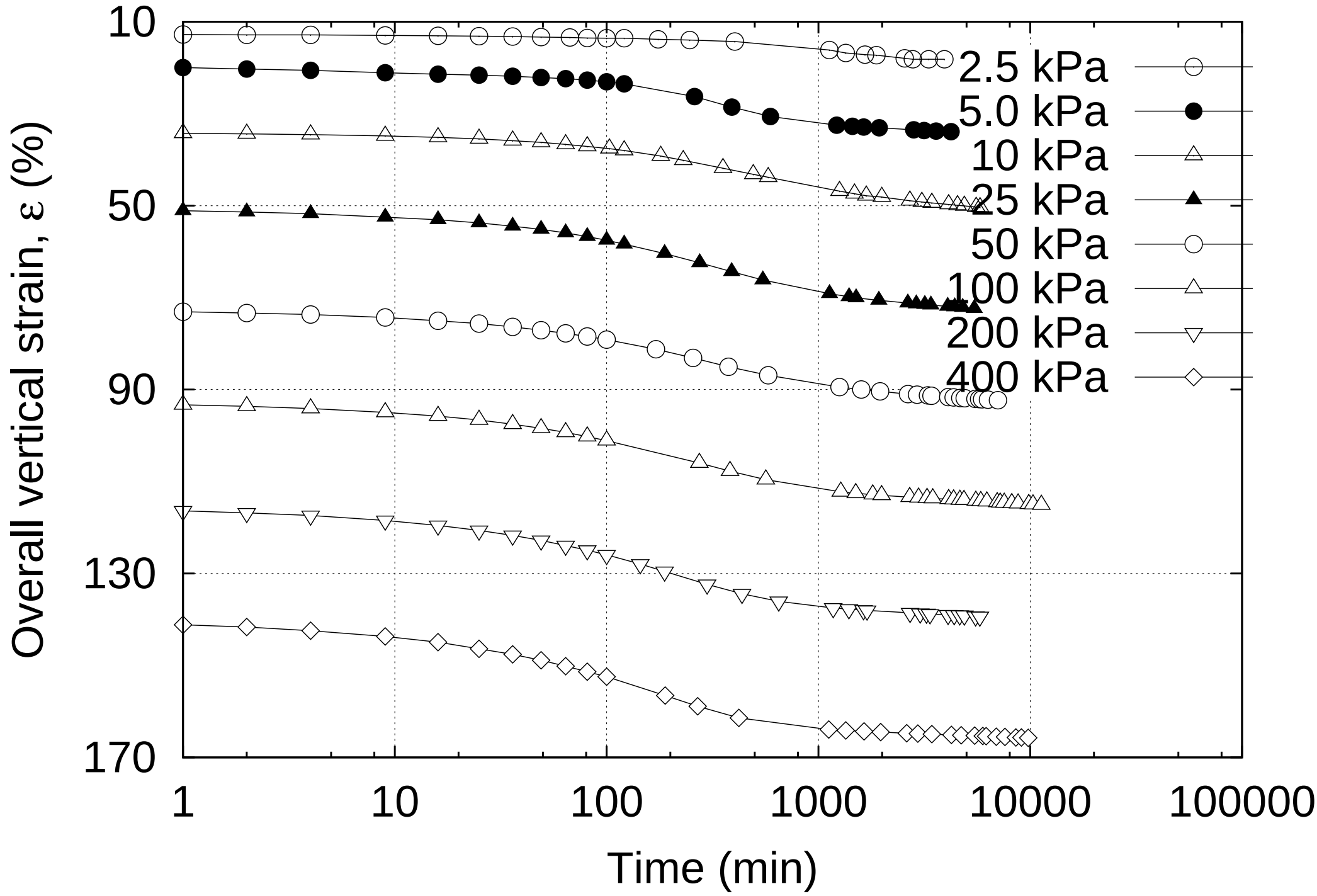

Figure1c

Click here to download Figure Figure1c.eps

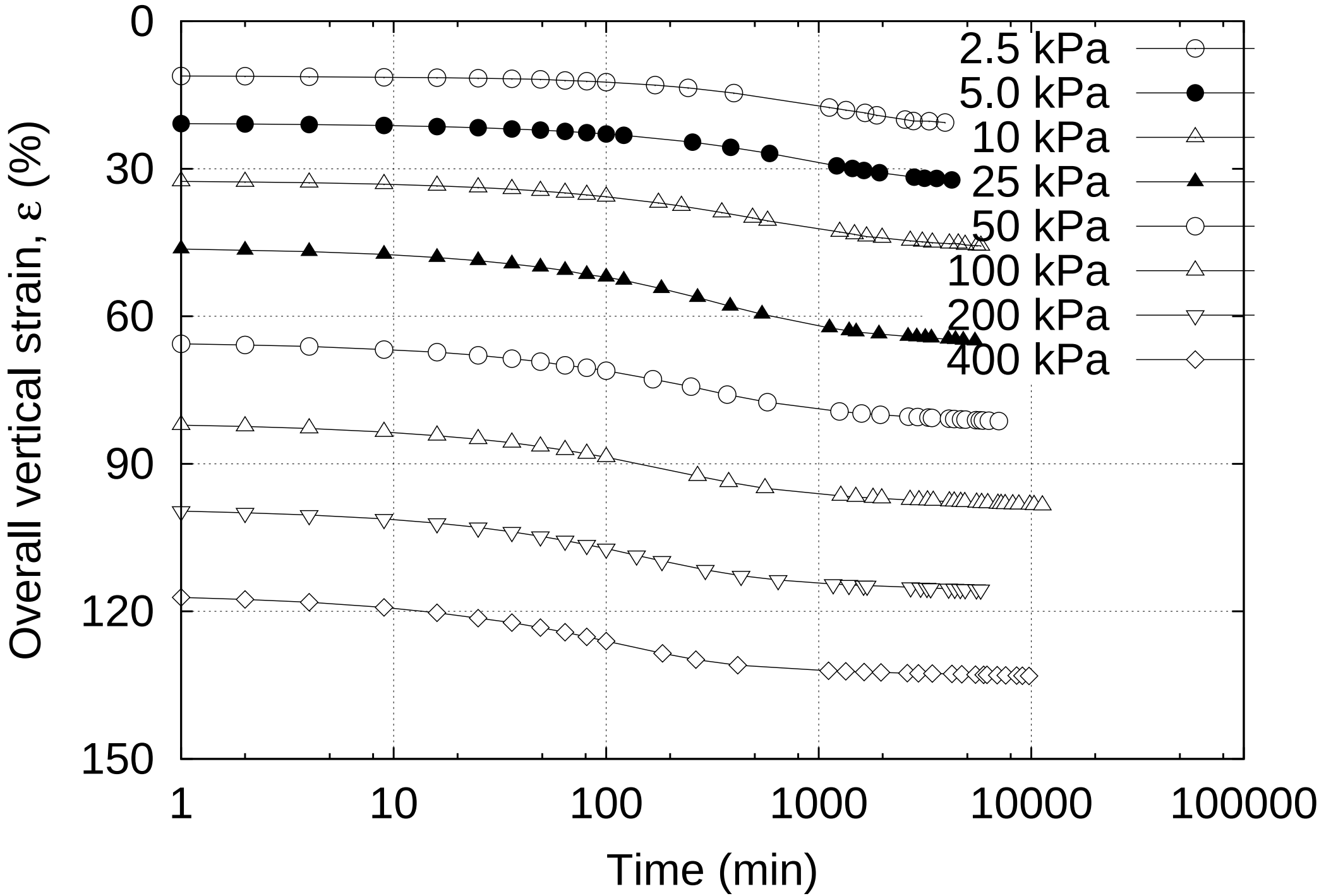

Figure1d

Click here to download Figure Figure1d.eps

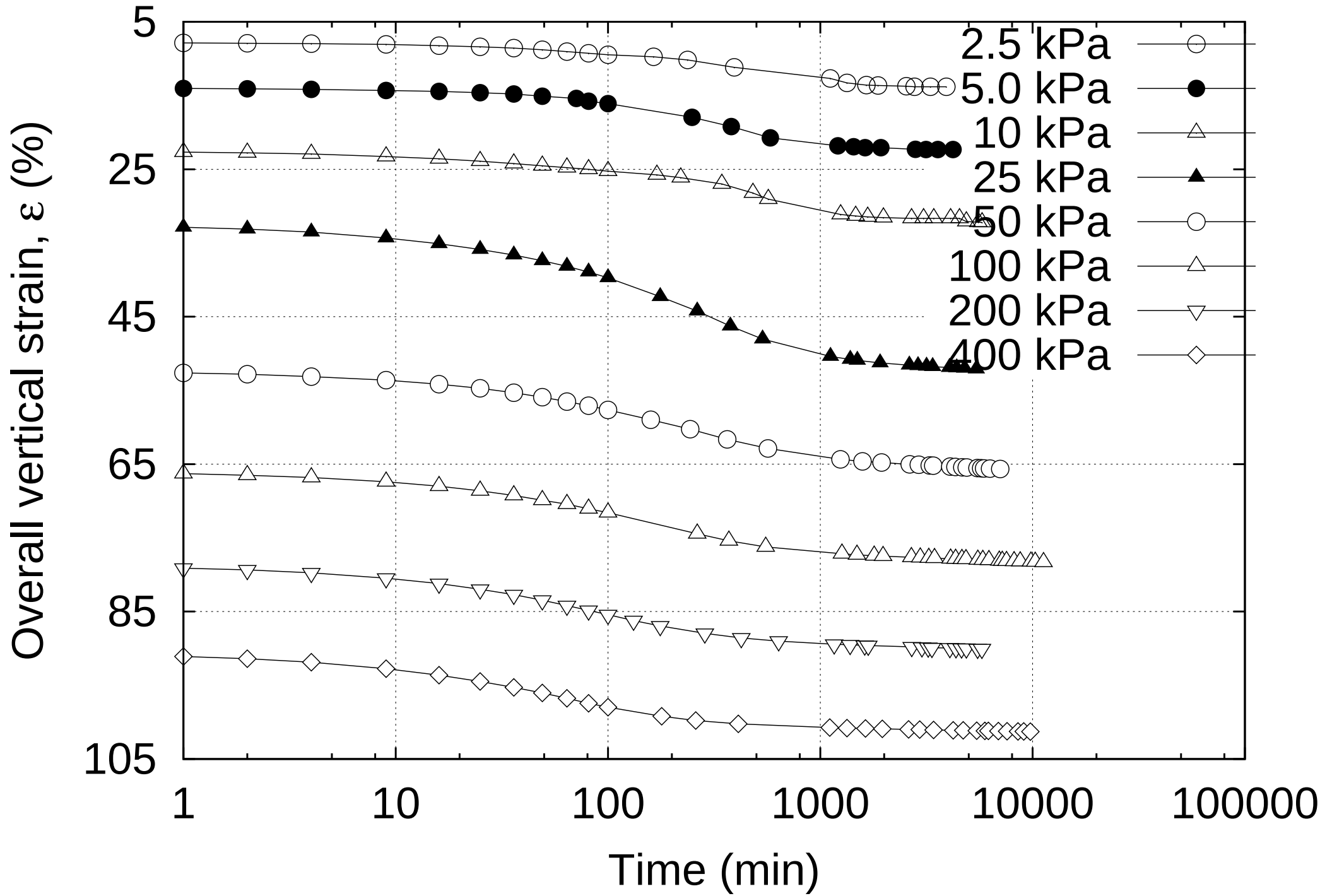

Figure1e

Click here to download Figure Figure1e.eps

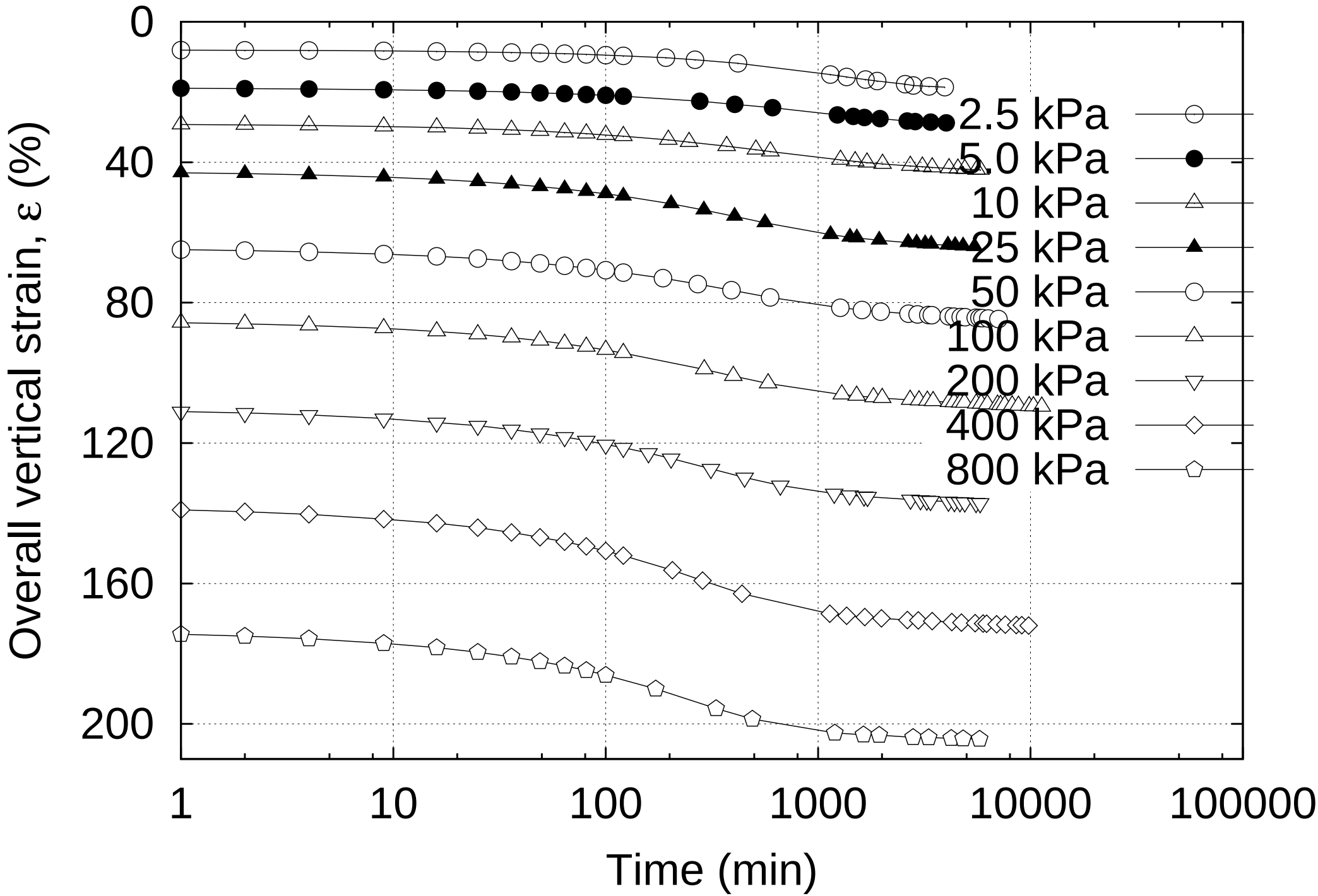

Figure1f

Click here to download Figure Figure1f.eps

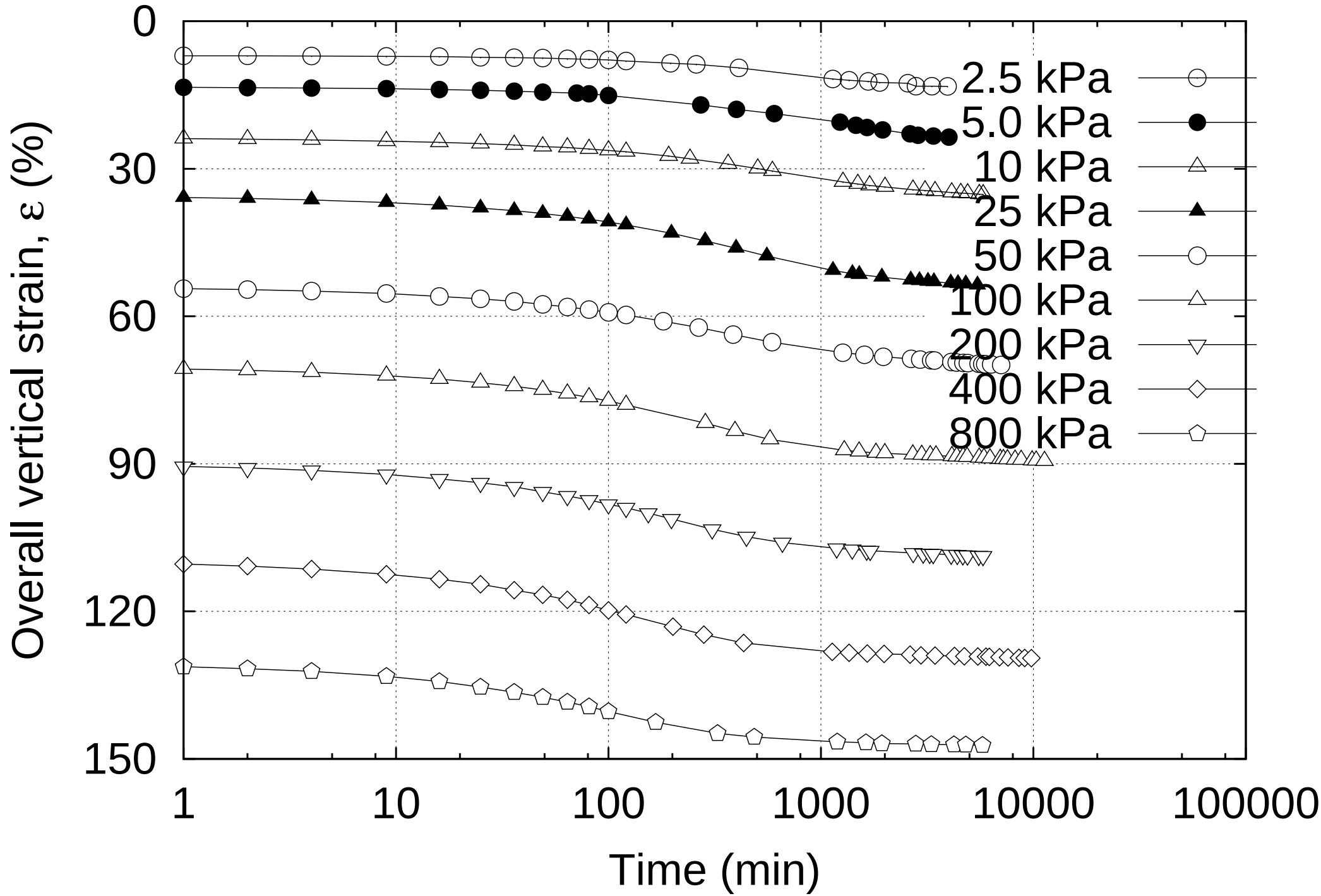

Figure1g

Click here to download Figure Figure1g.eps

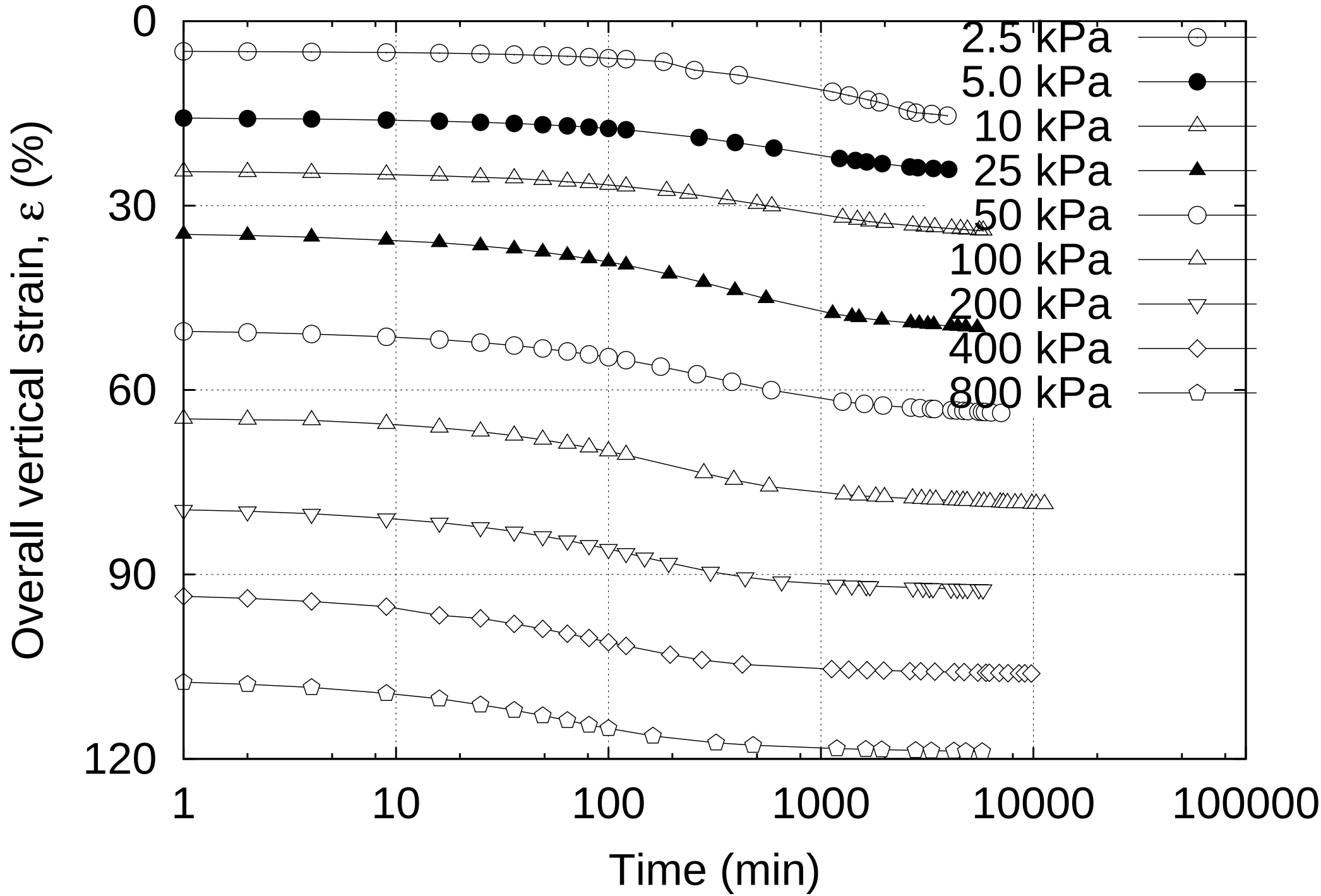

Figure2a

Click here to download Figure Figure2a.eps

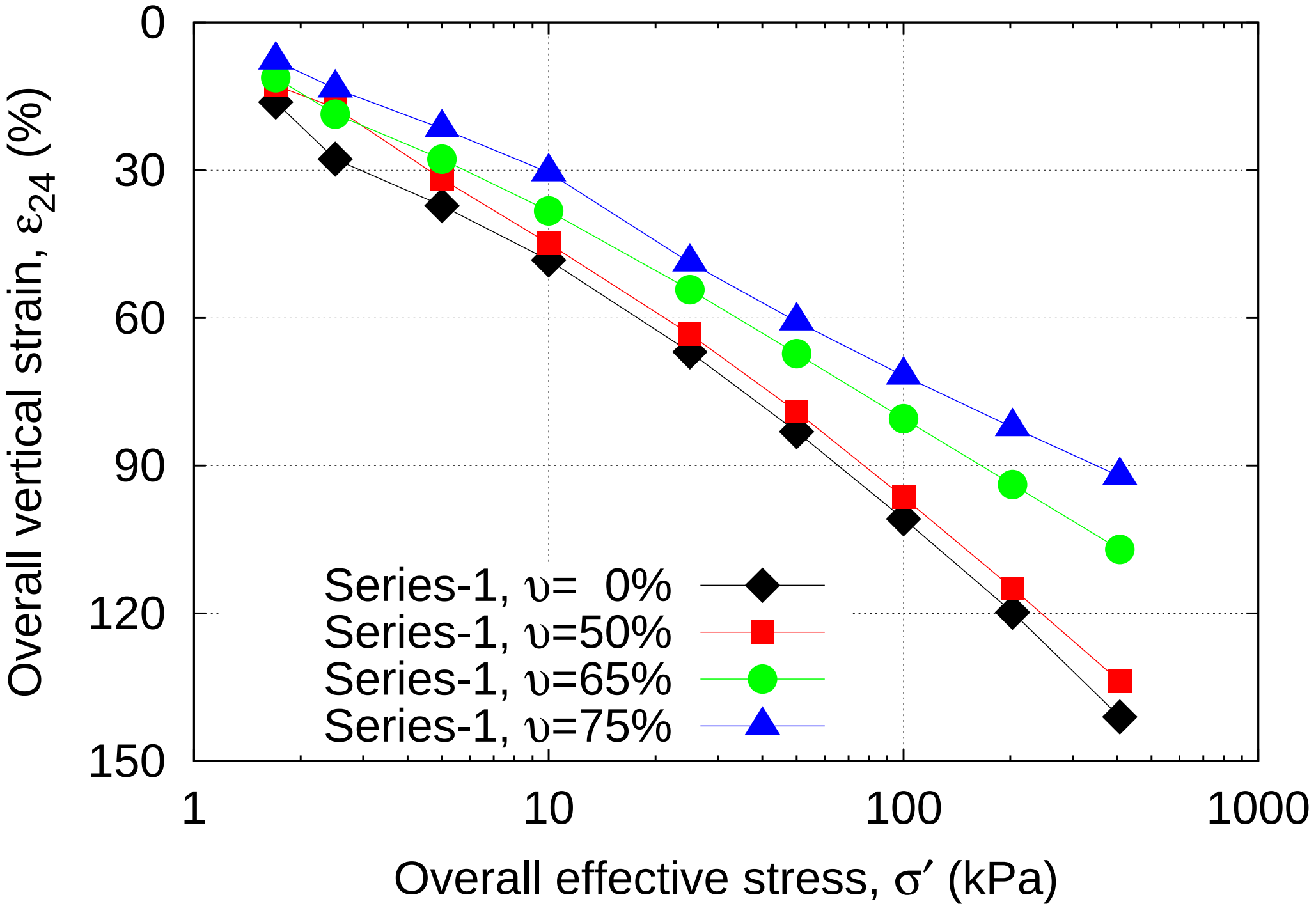

Figure2b

Click here to download Figure Figure2b.eps

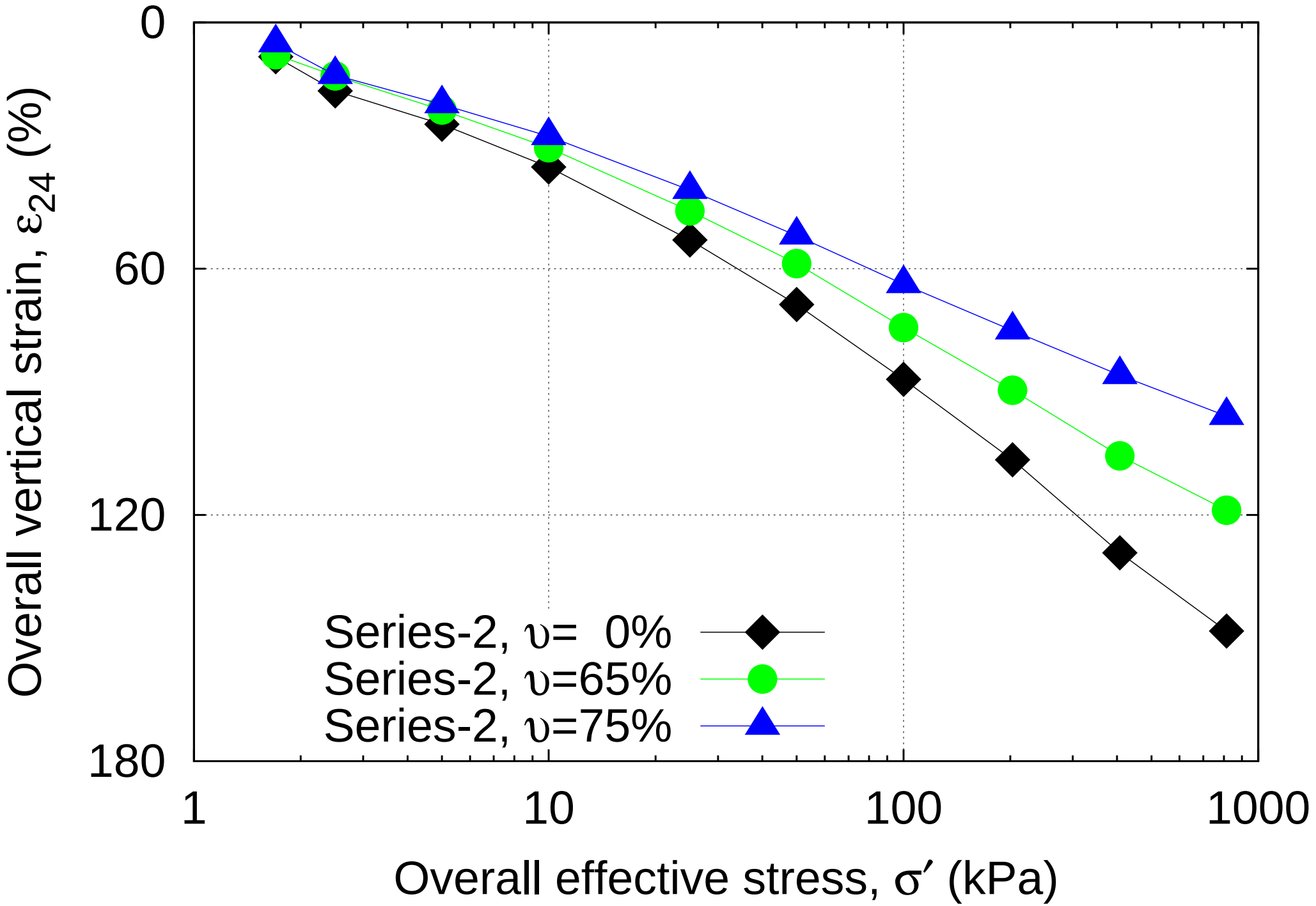

Figure3a

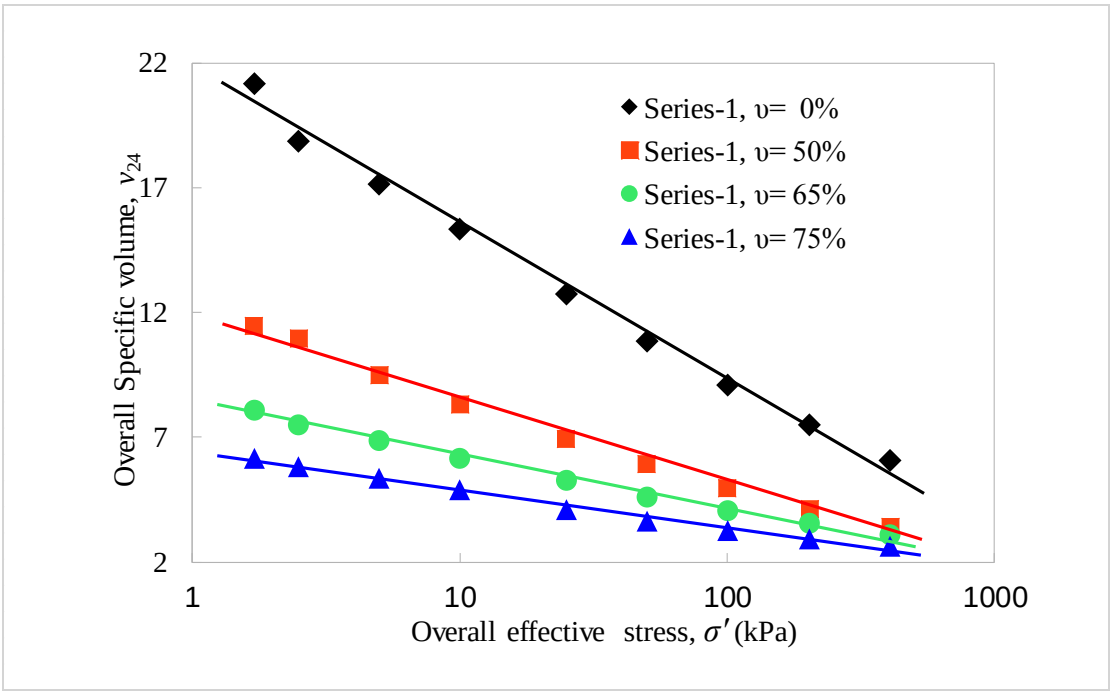

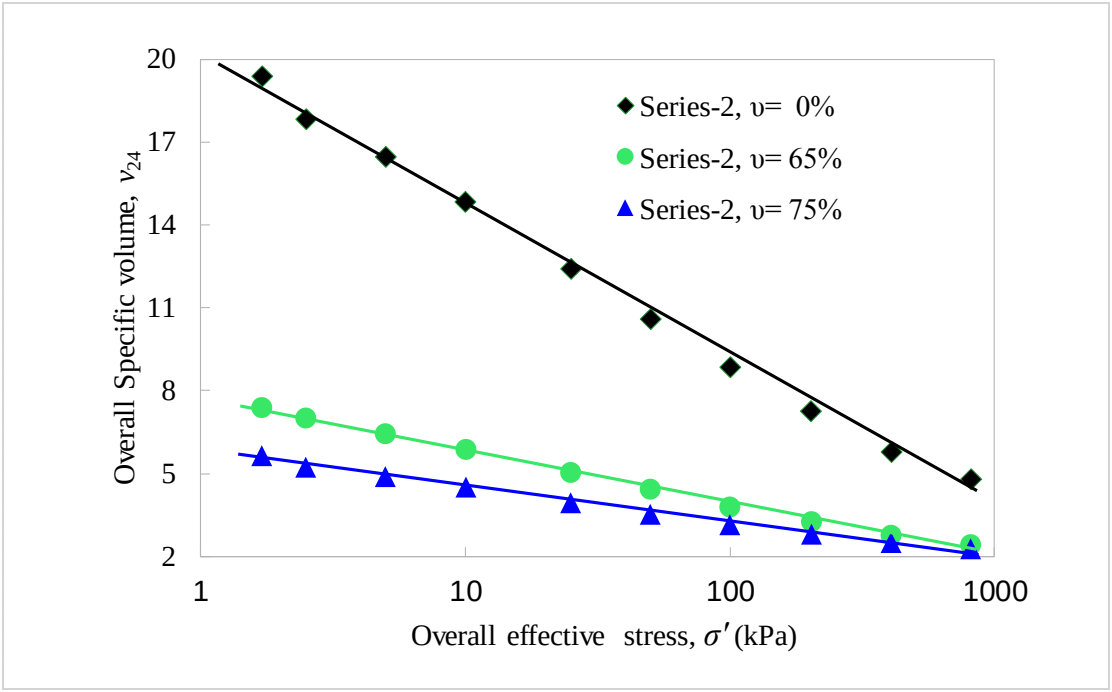

Figure4a

Click here to download Figure Figure4a.eps

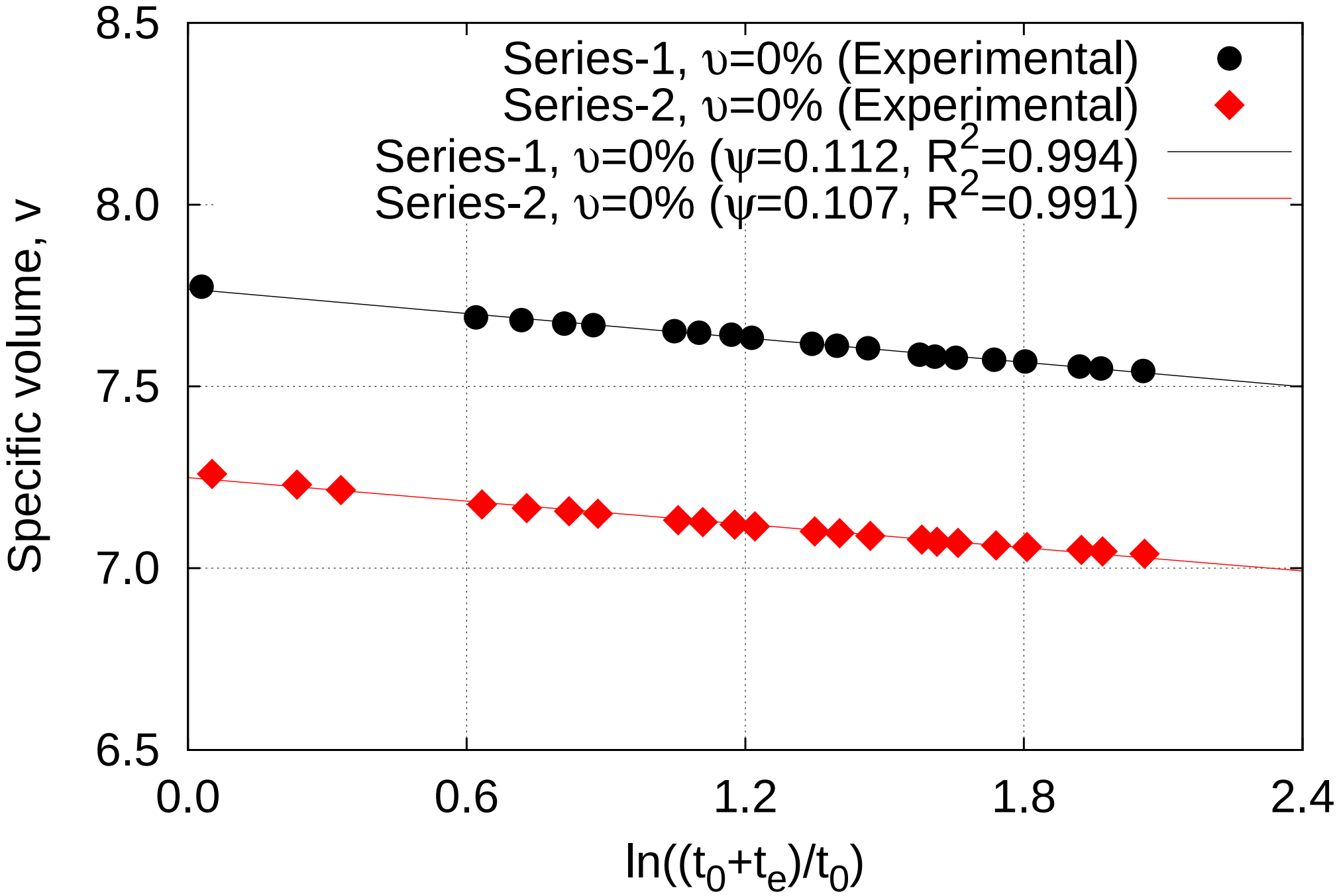

Figure4b

Click here to download Figure Figure4b.eps

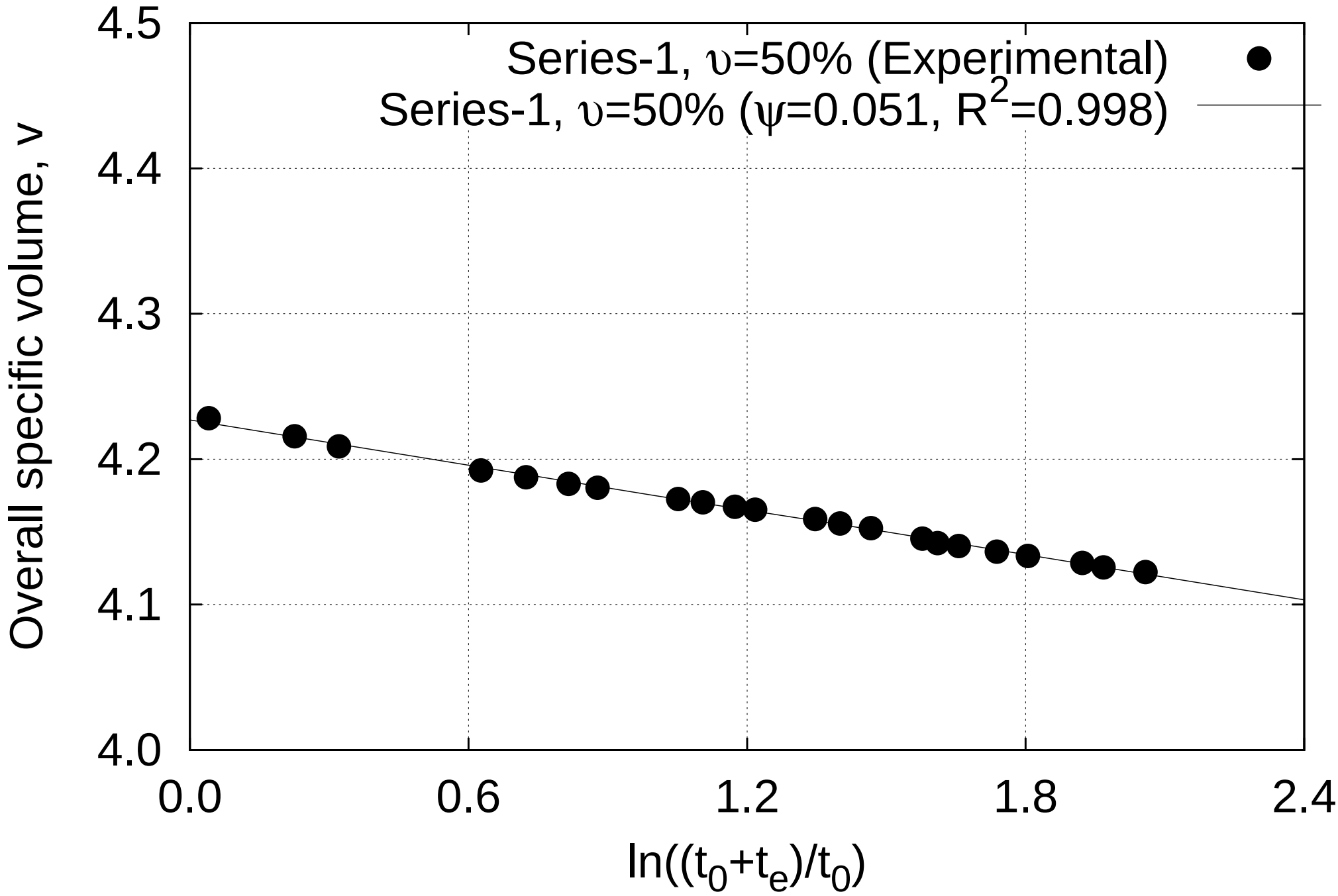

Figure4c

Click here to download Figure Figure4c.eps

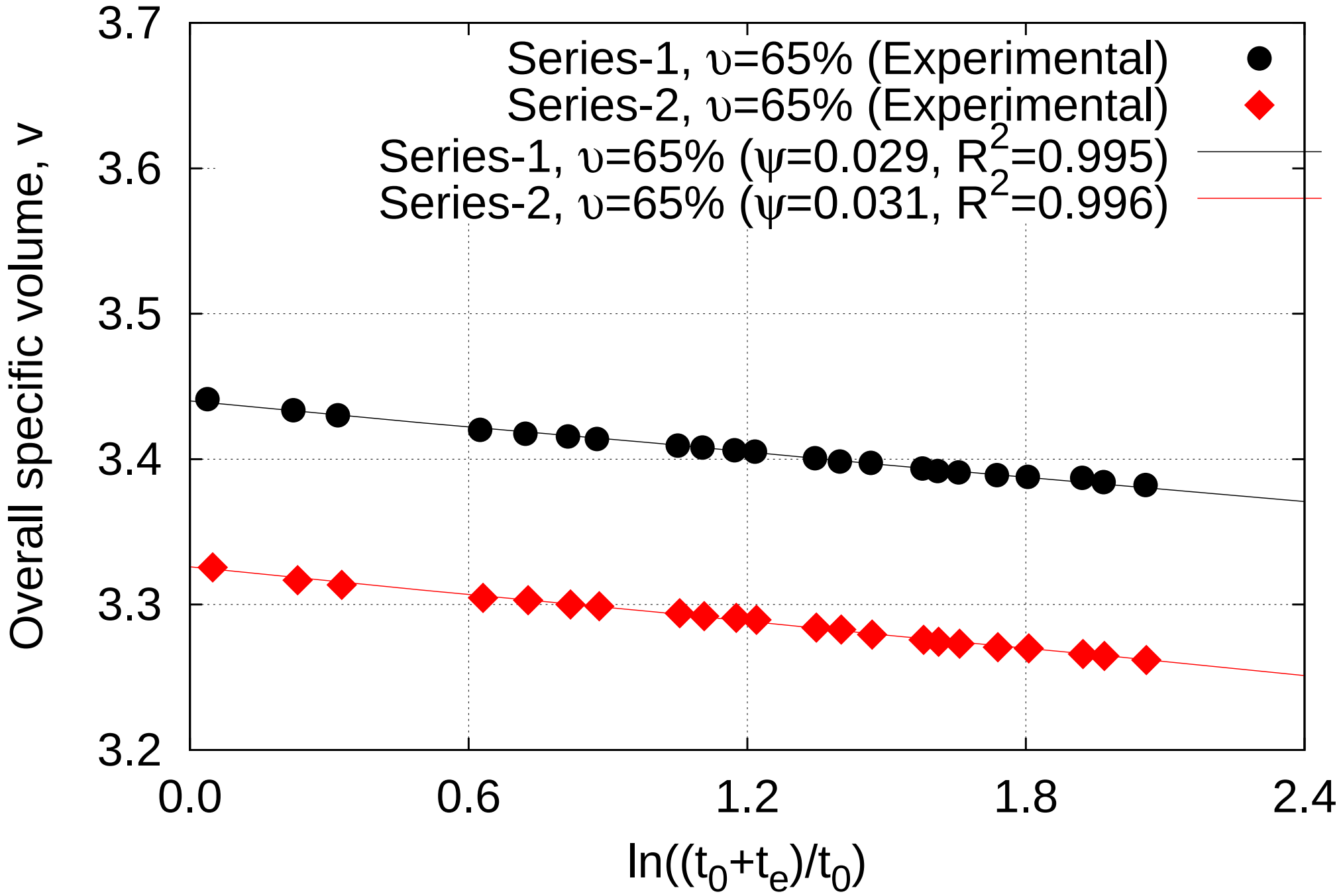

Figure4d

Click here to download Figure Figure4d.eps

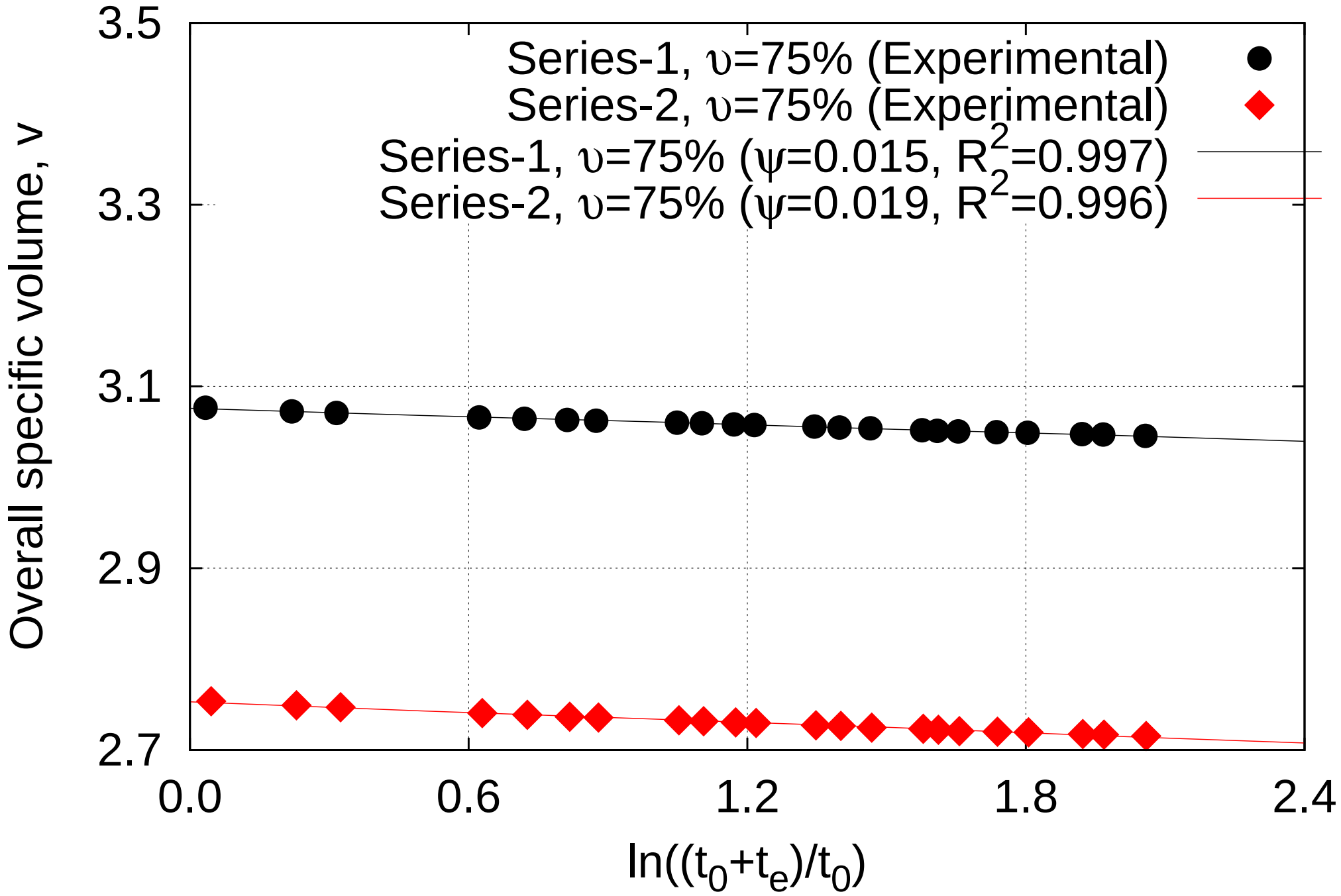

Figure5

Click here to download Figure Figure5.eps

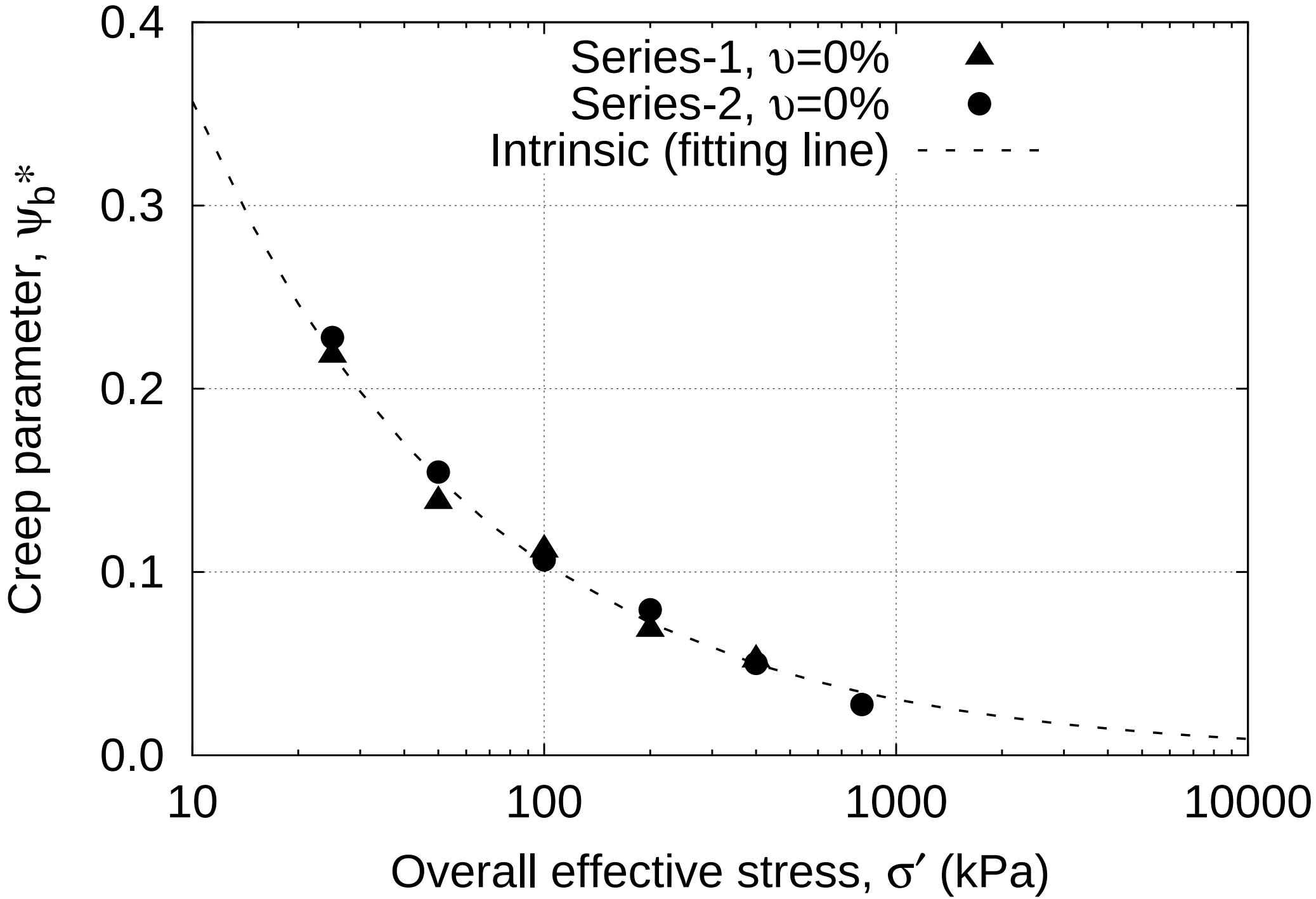

Figure6a

Click here to download Figure Figure6a.eps

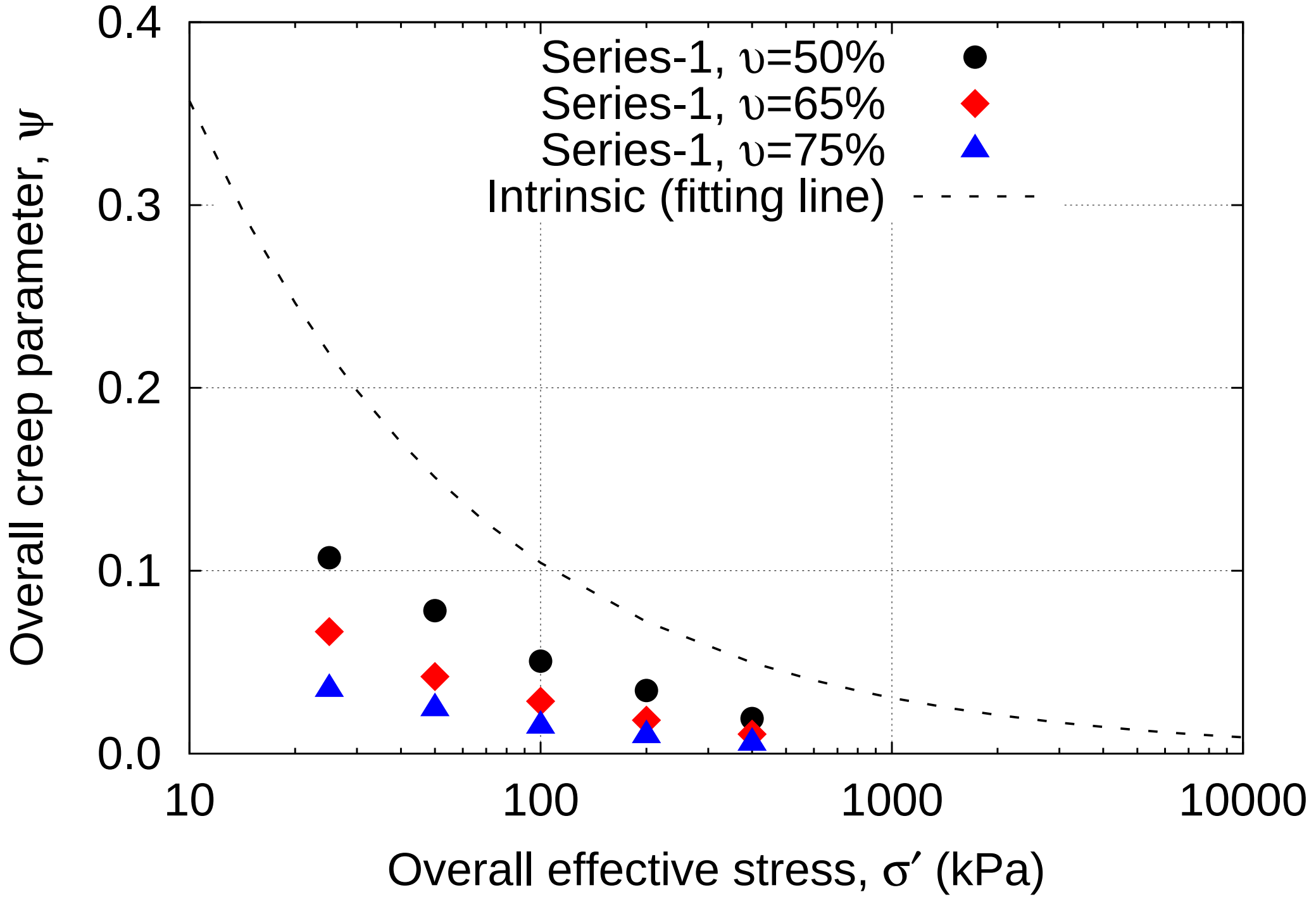

Figure6b

Click here to download Figure Figure6b.eps

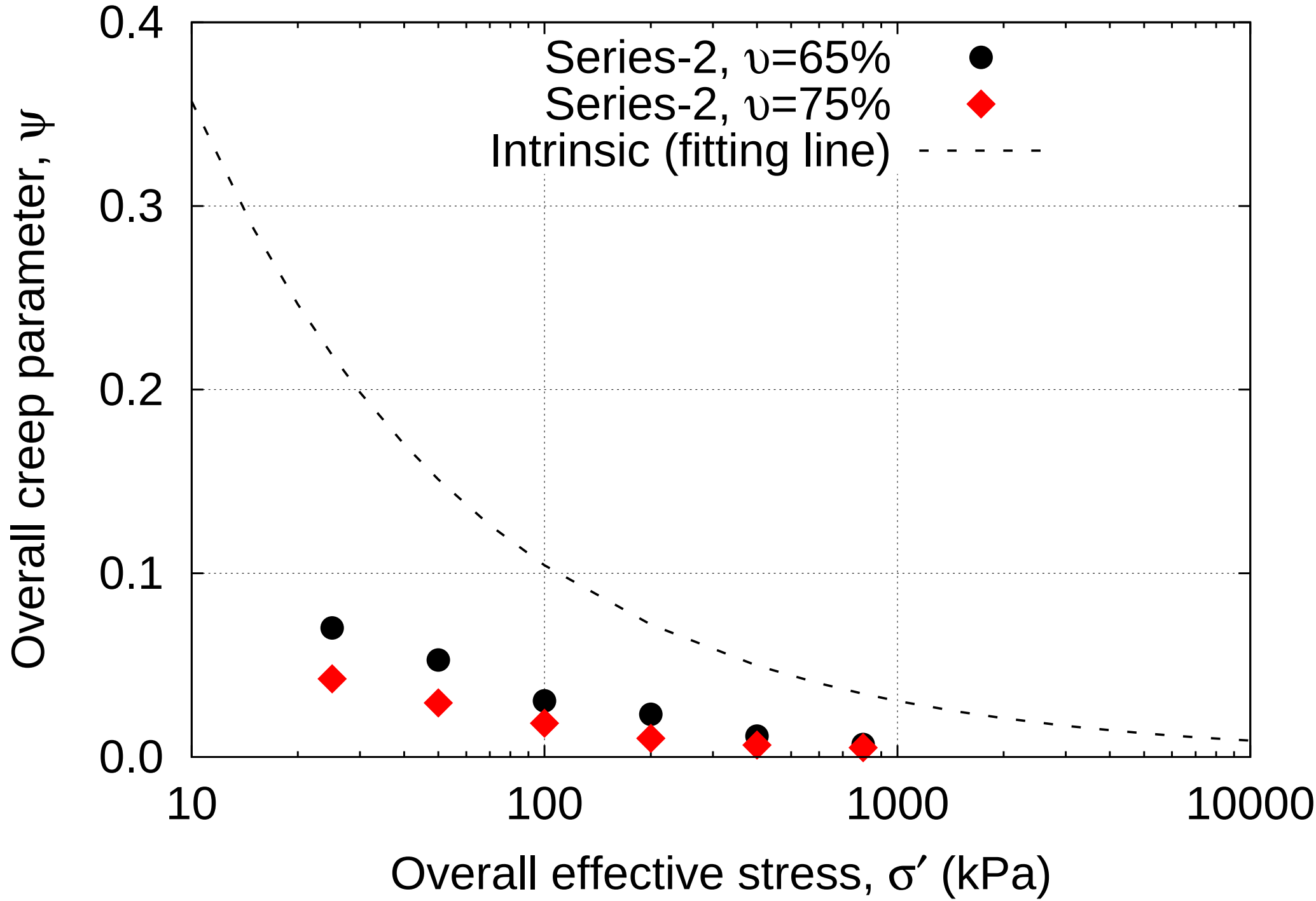

Figure7a

Click here to download Figure Figure7a.eps

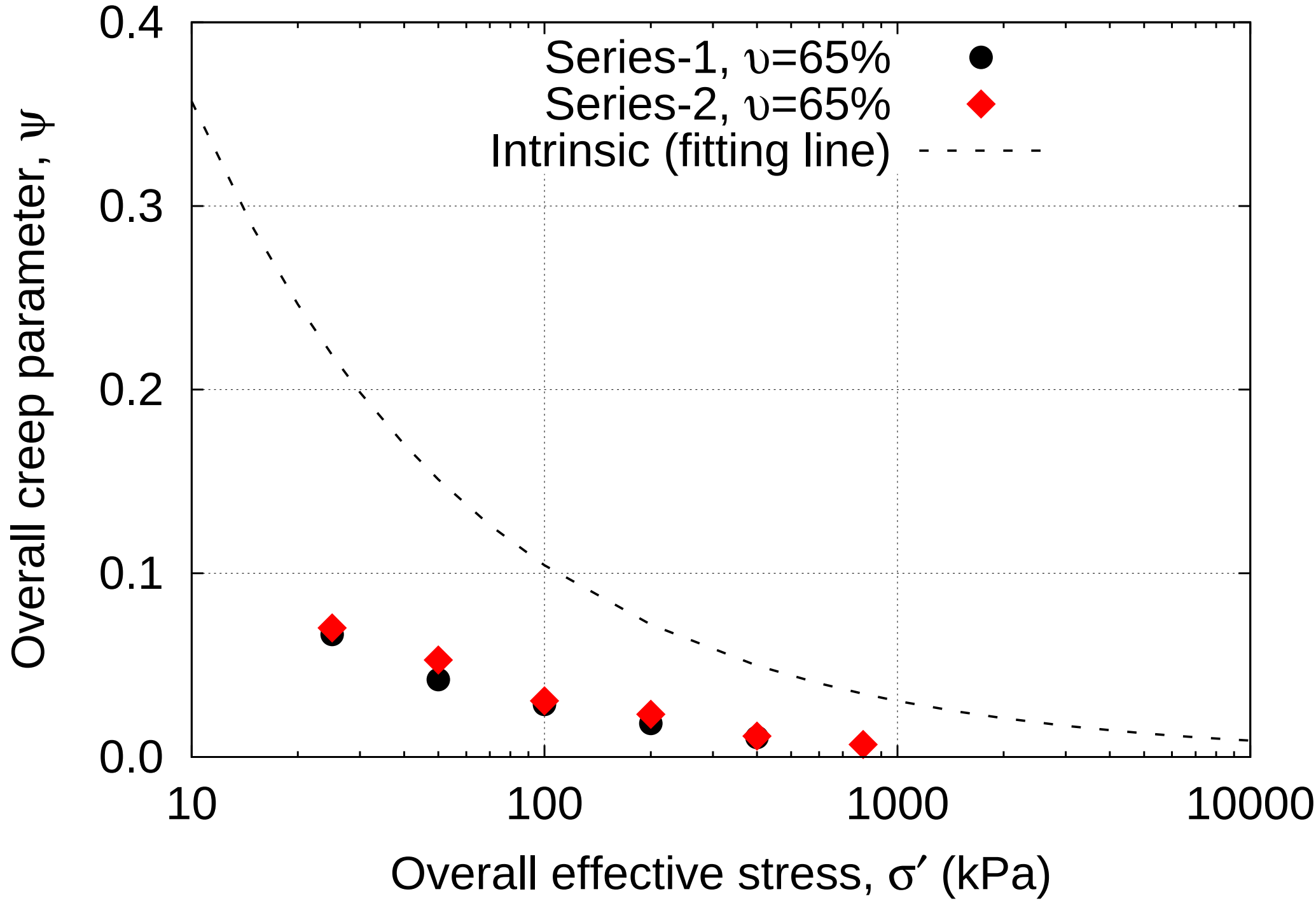

Figure7b

Click here to download Figure Figure7b.eps

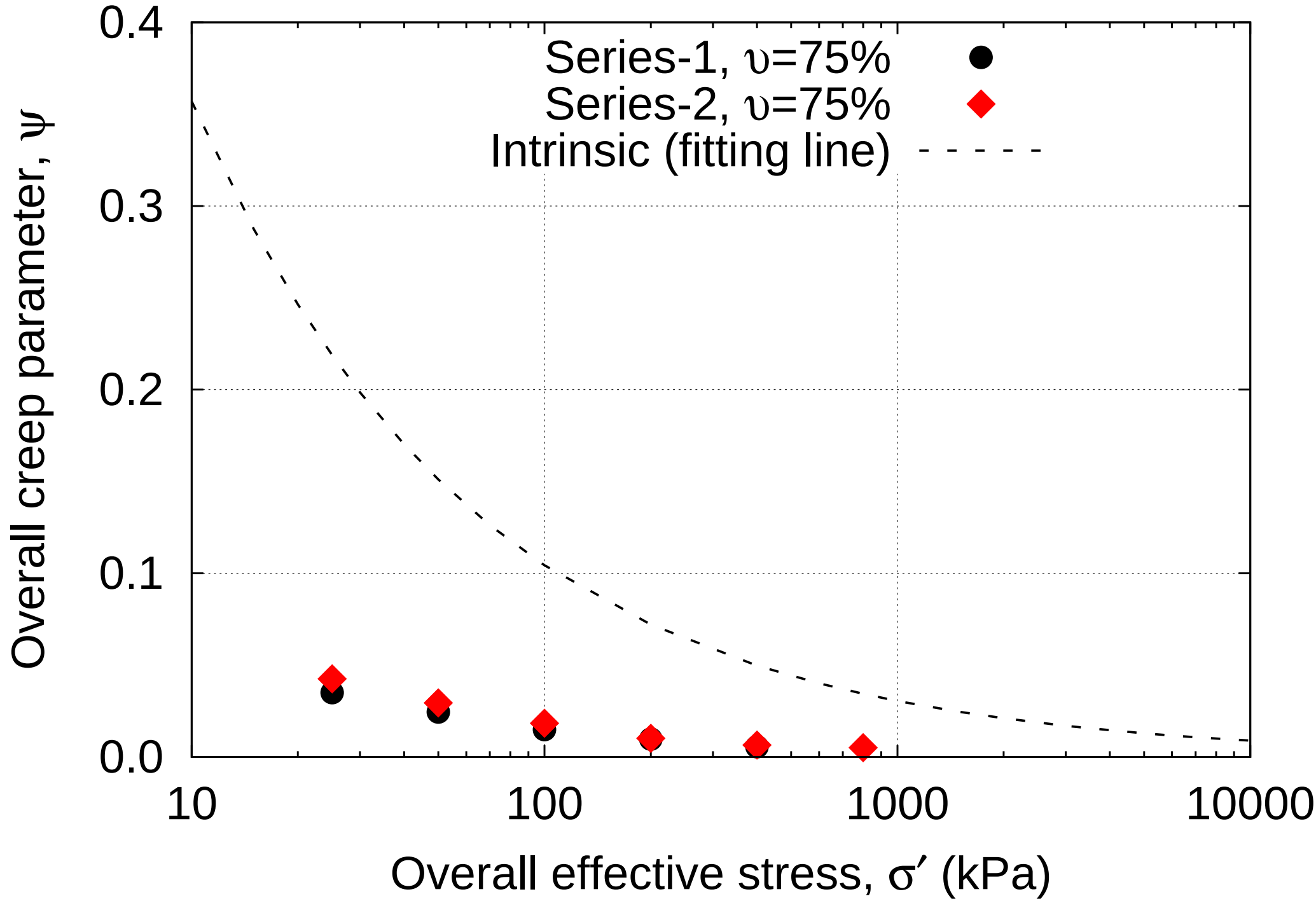

Figure8a

Click here to download Figure Figure8a.eps

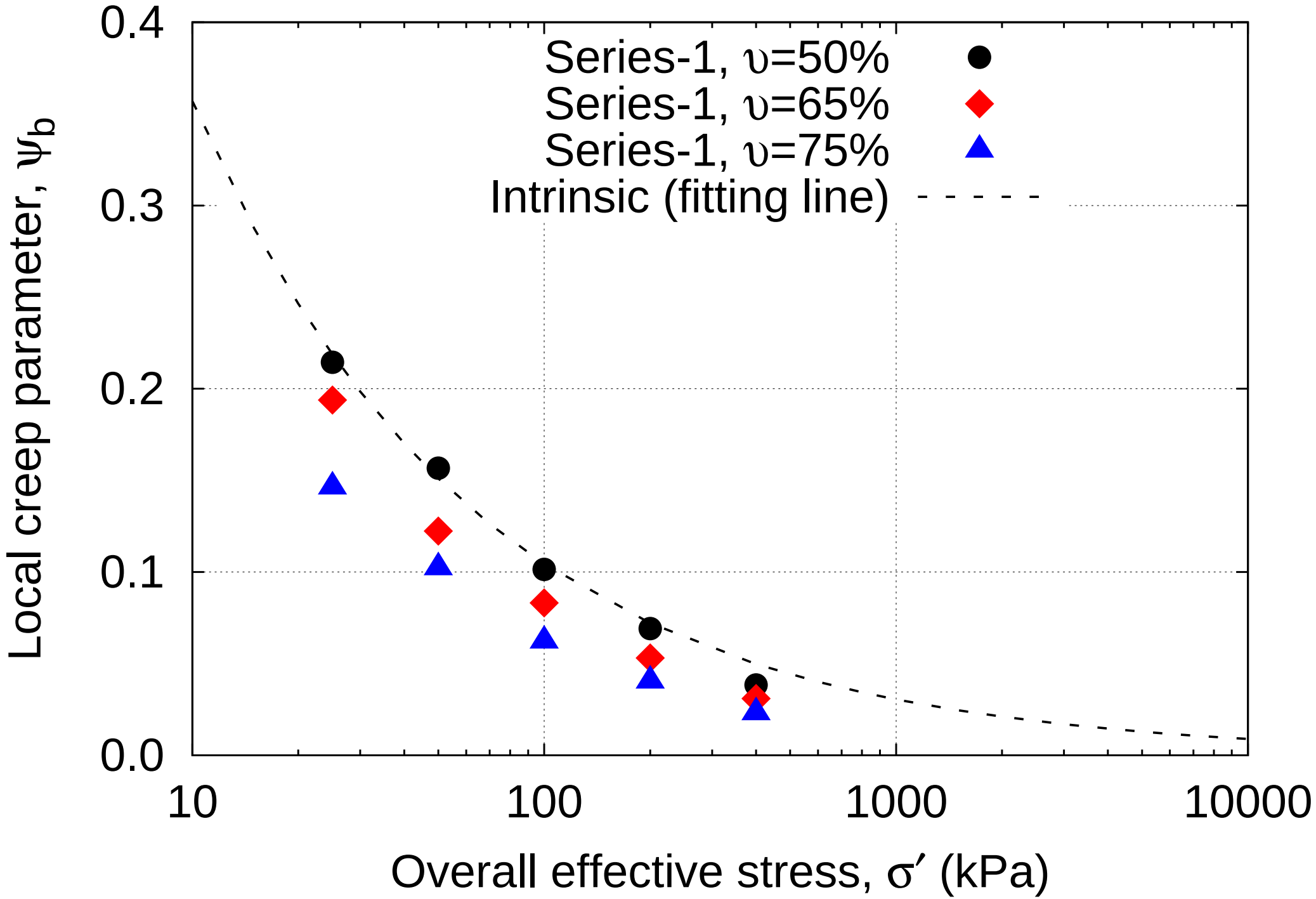

Figure8b

Click here to download Figure Figure8b.eps

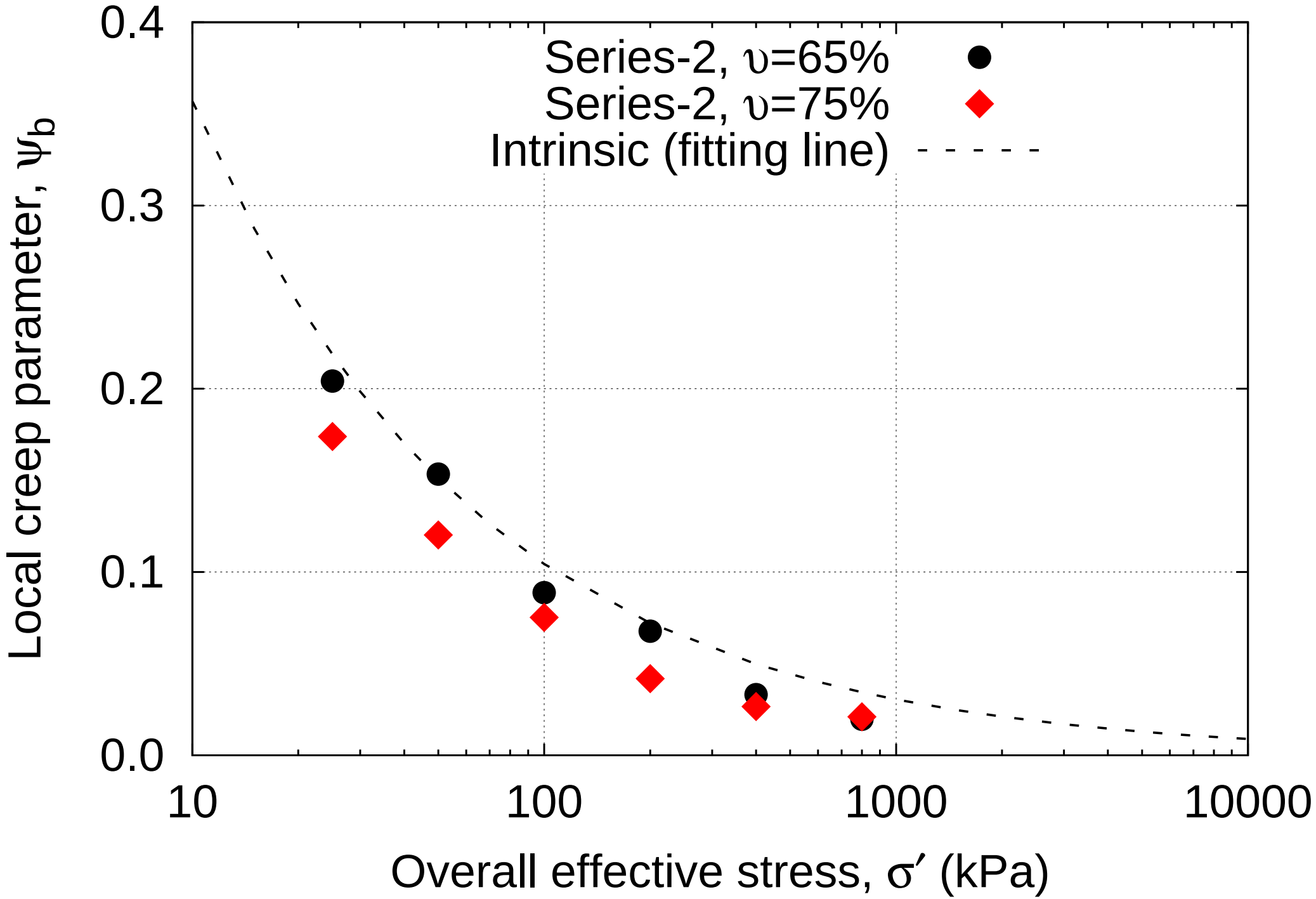

Figure9a

Click here to download Figure Figure9a.eps

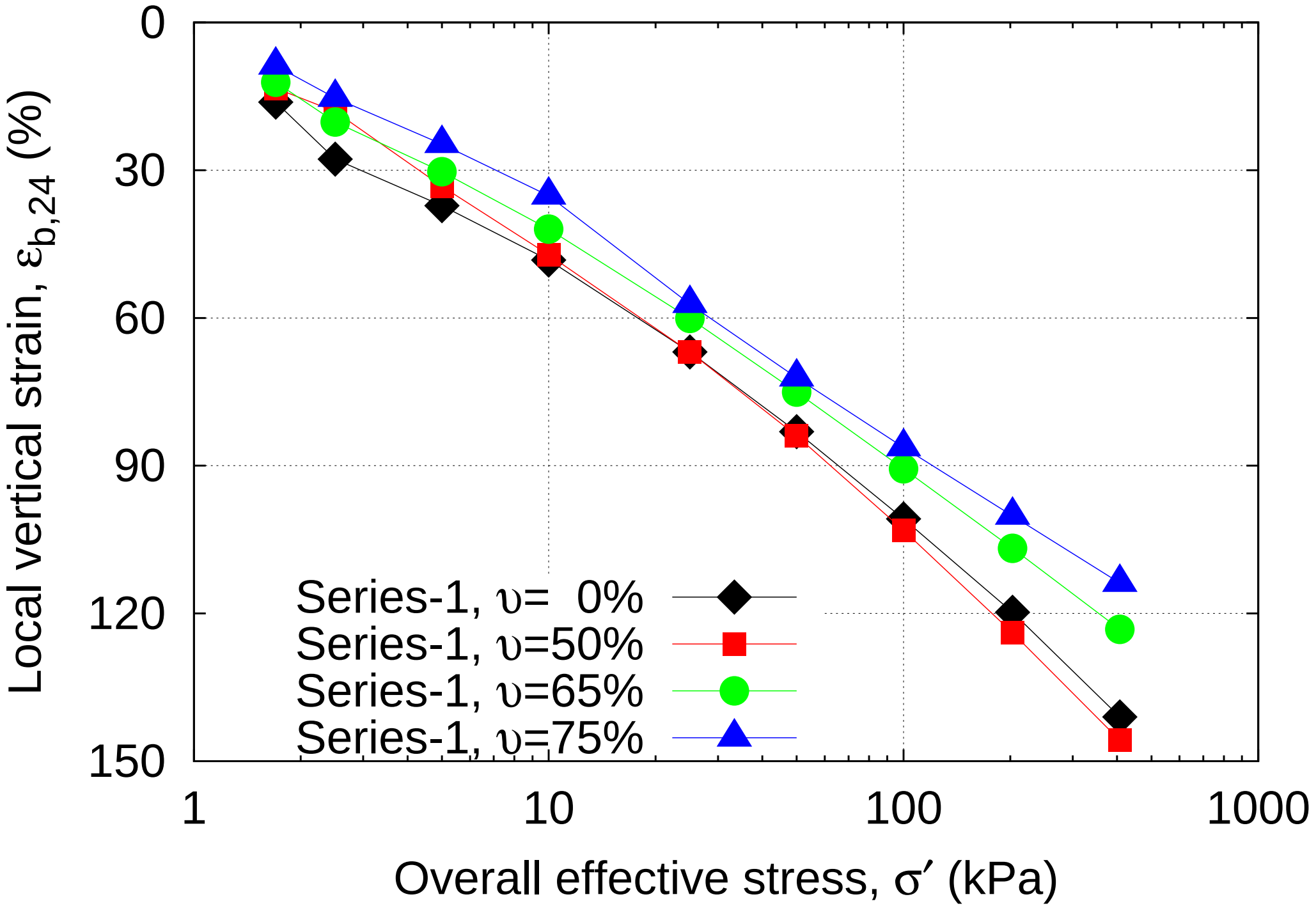

Figure9b

Click here to download Figure Figure9b.eps

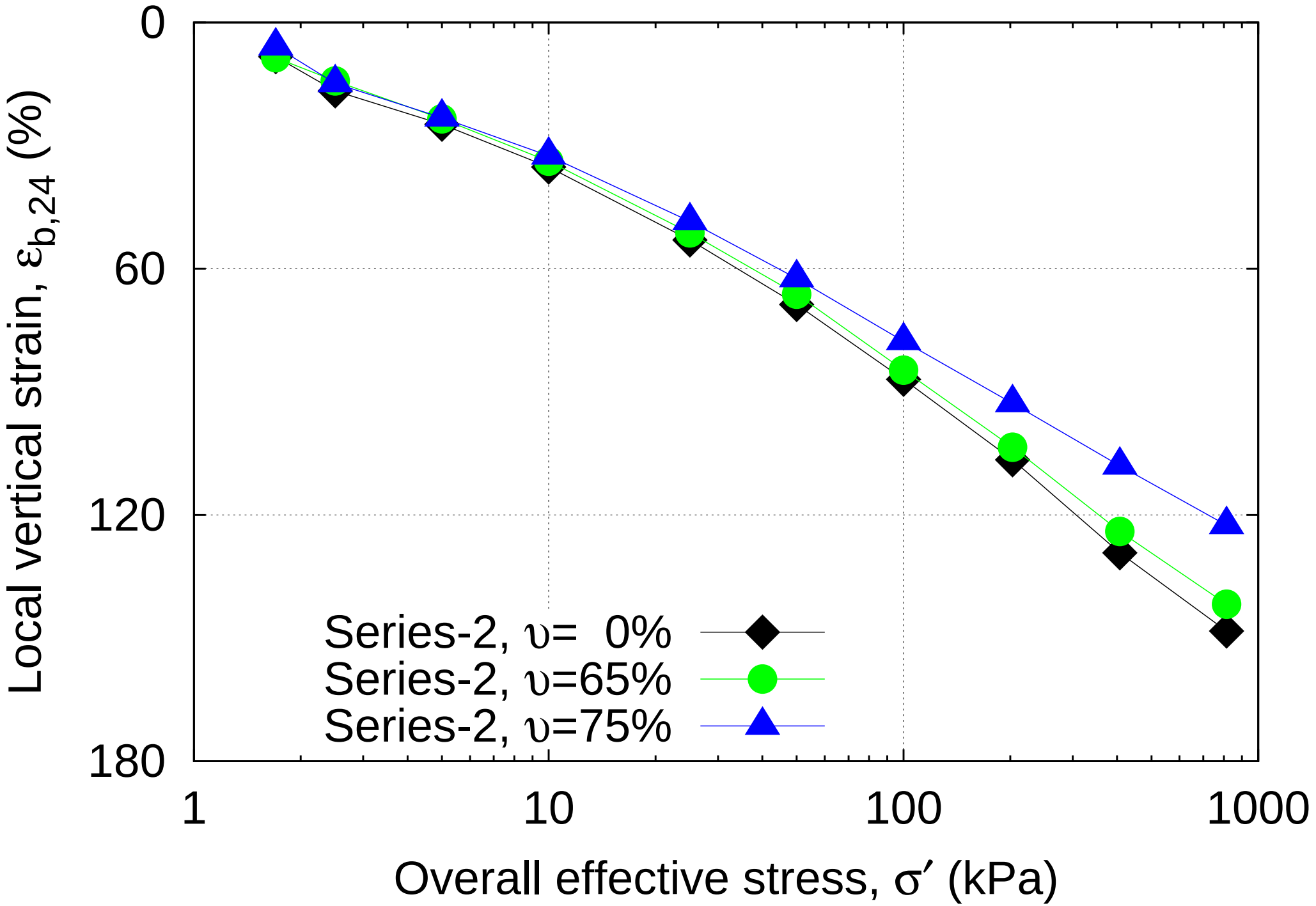

Figure10

Click here to download Figure Figure10.eps

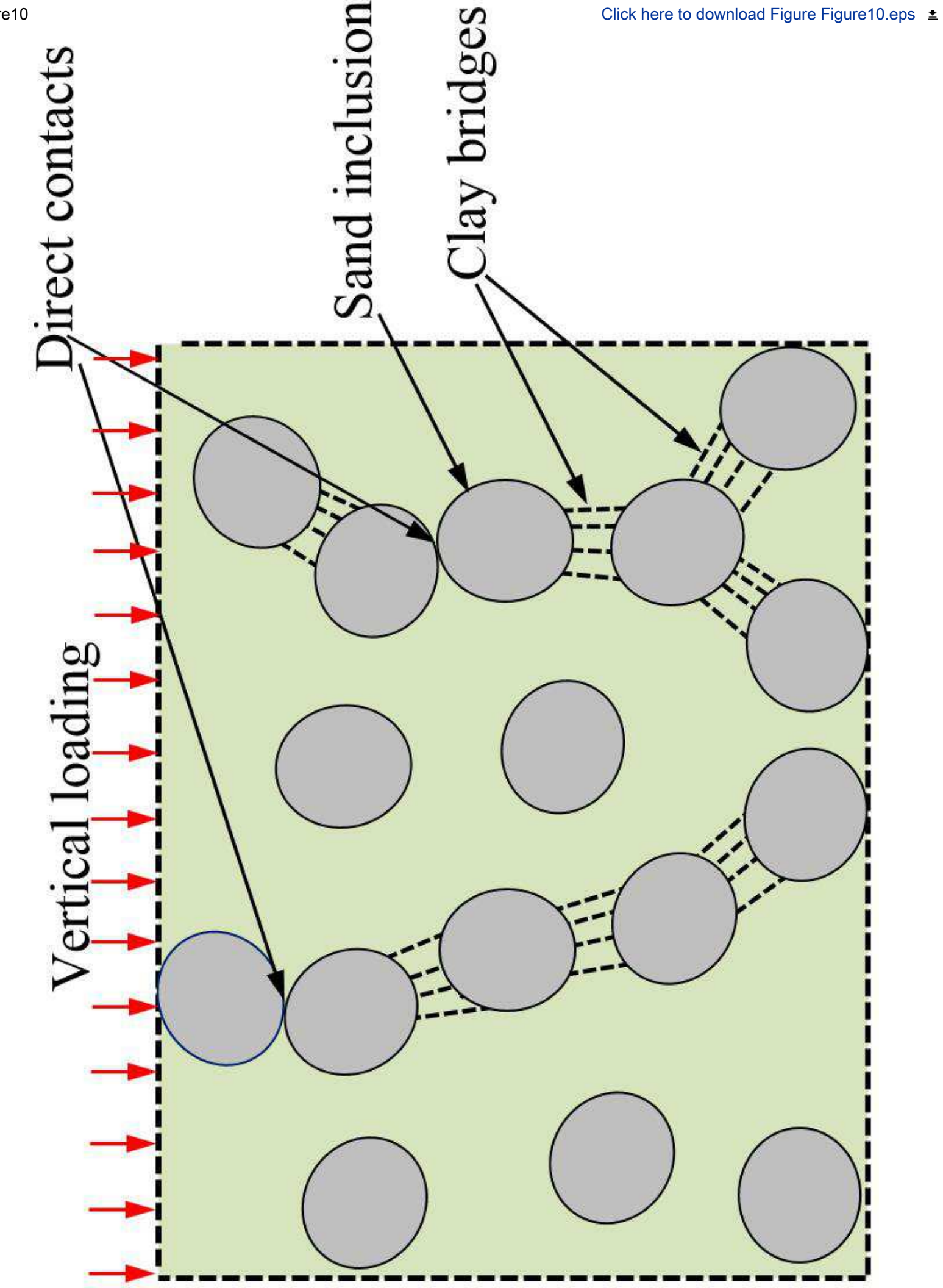

Figure11

Click here to download Figure Figure11.eps

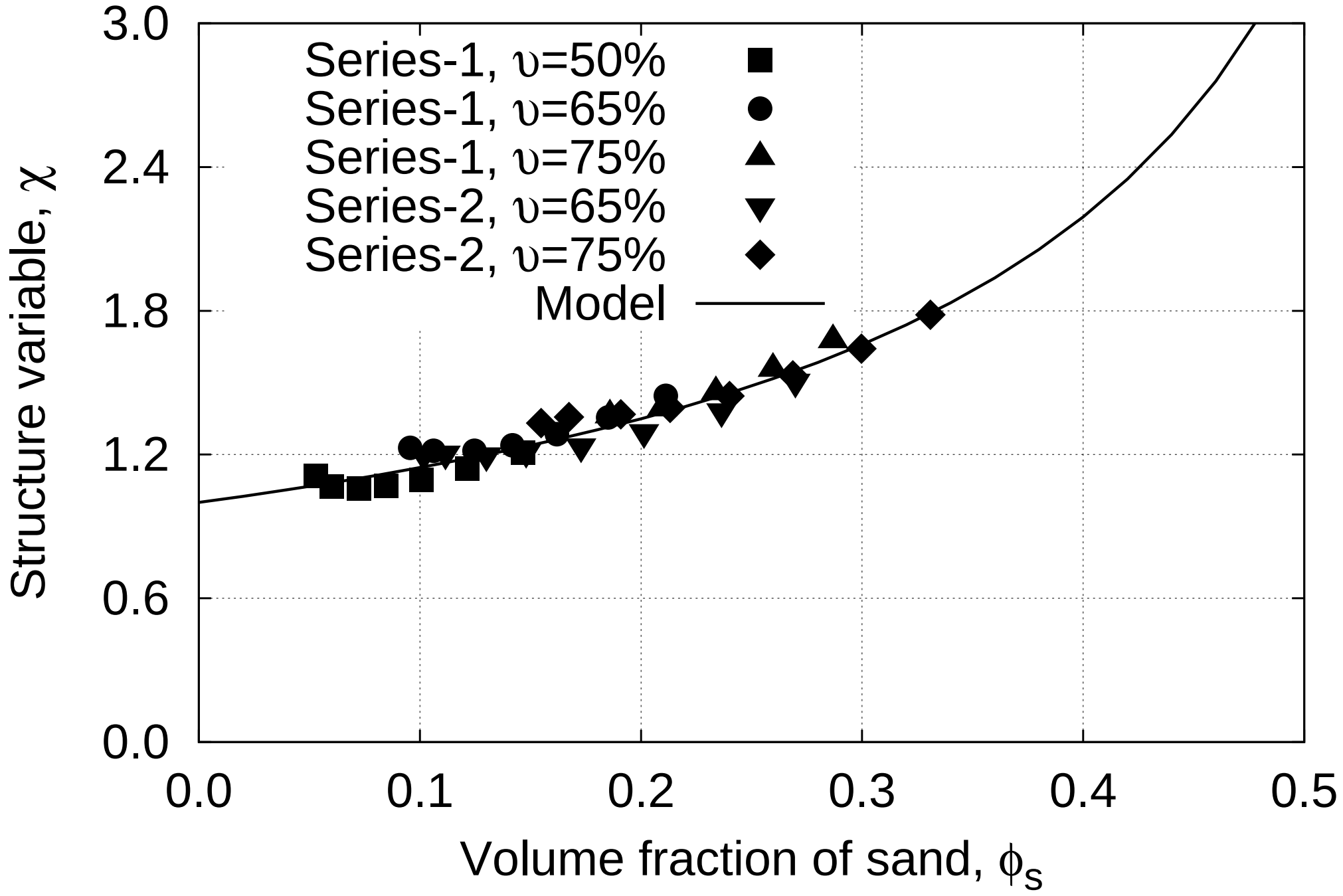

Figure12

Click here to download Figure Figure12.eps

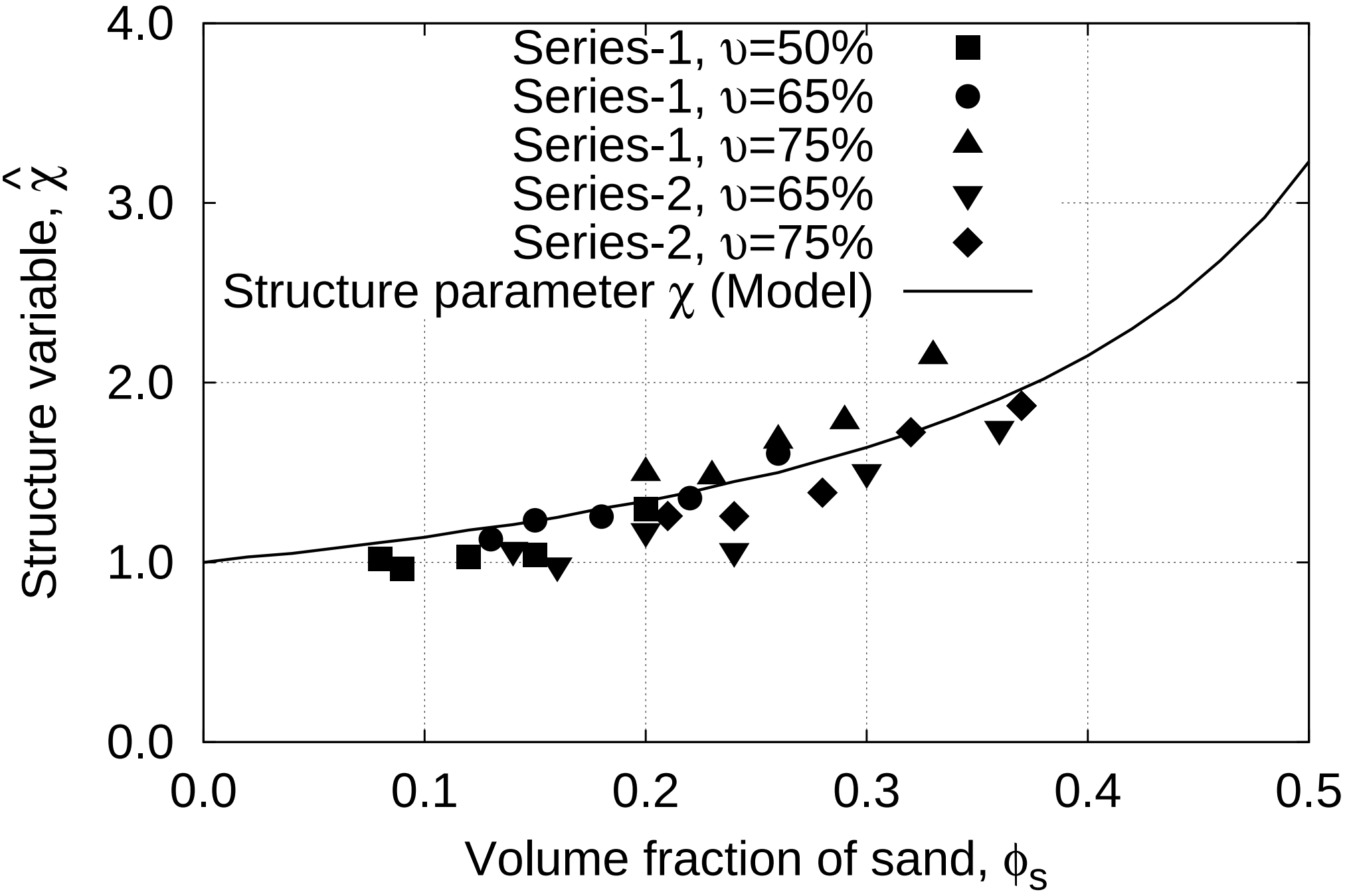

Figure13a

Click here to download Figure Figure13a.eps

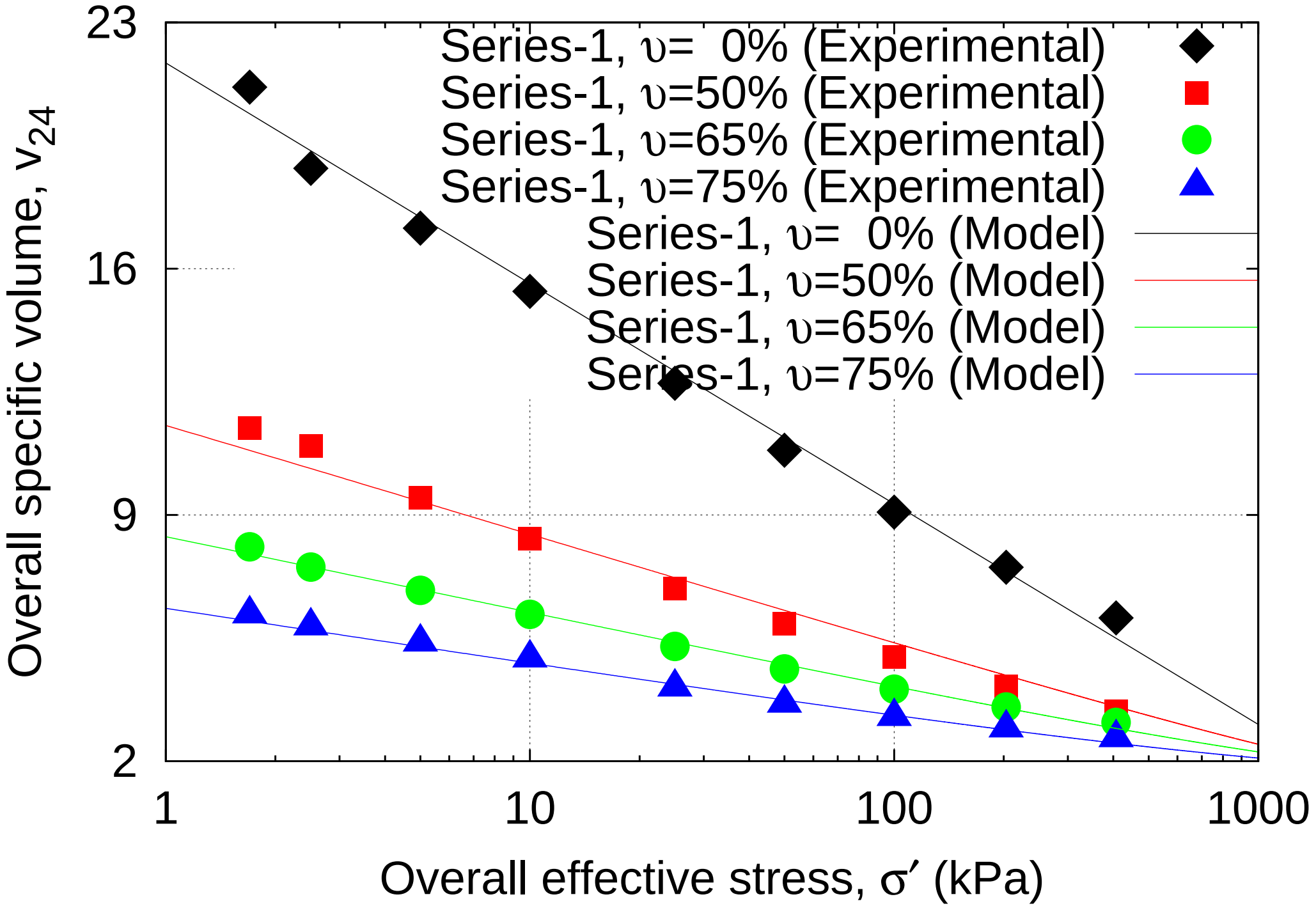

Figure13b

Click here to download Figure Figure13b.eps

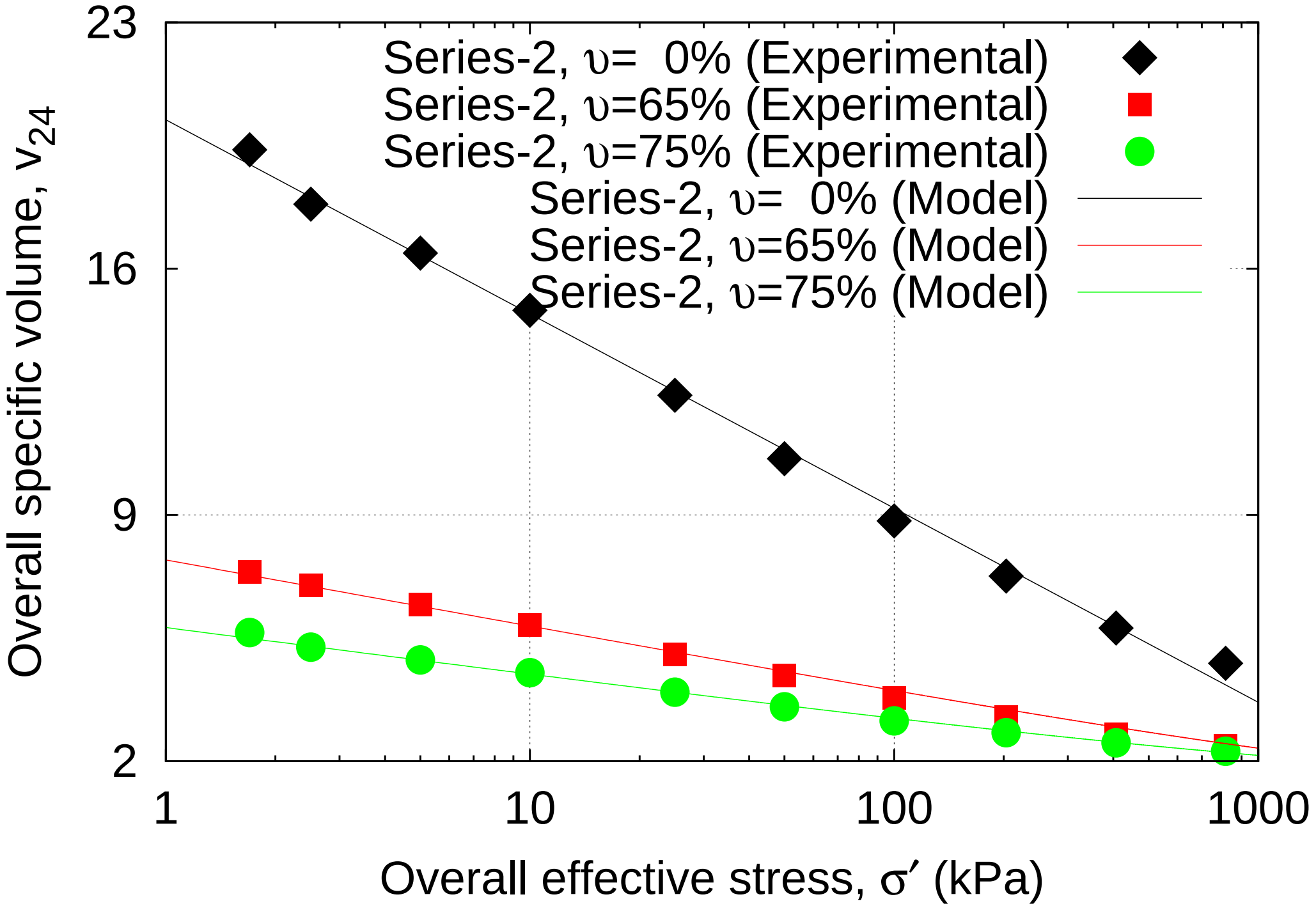

Figure14a

Click here to download Figure Figure14a.eps

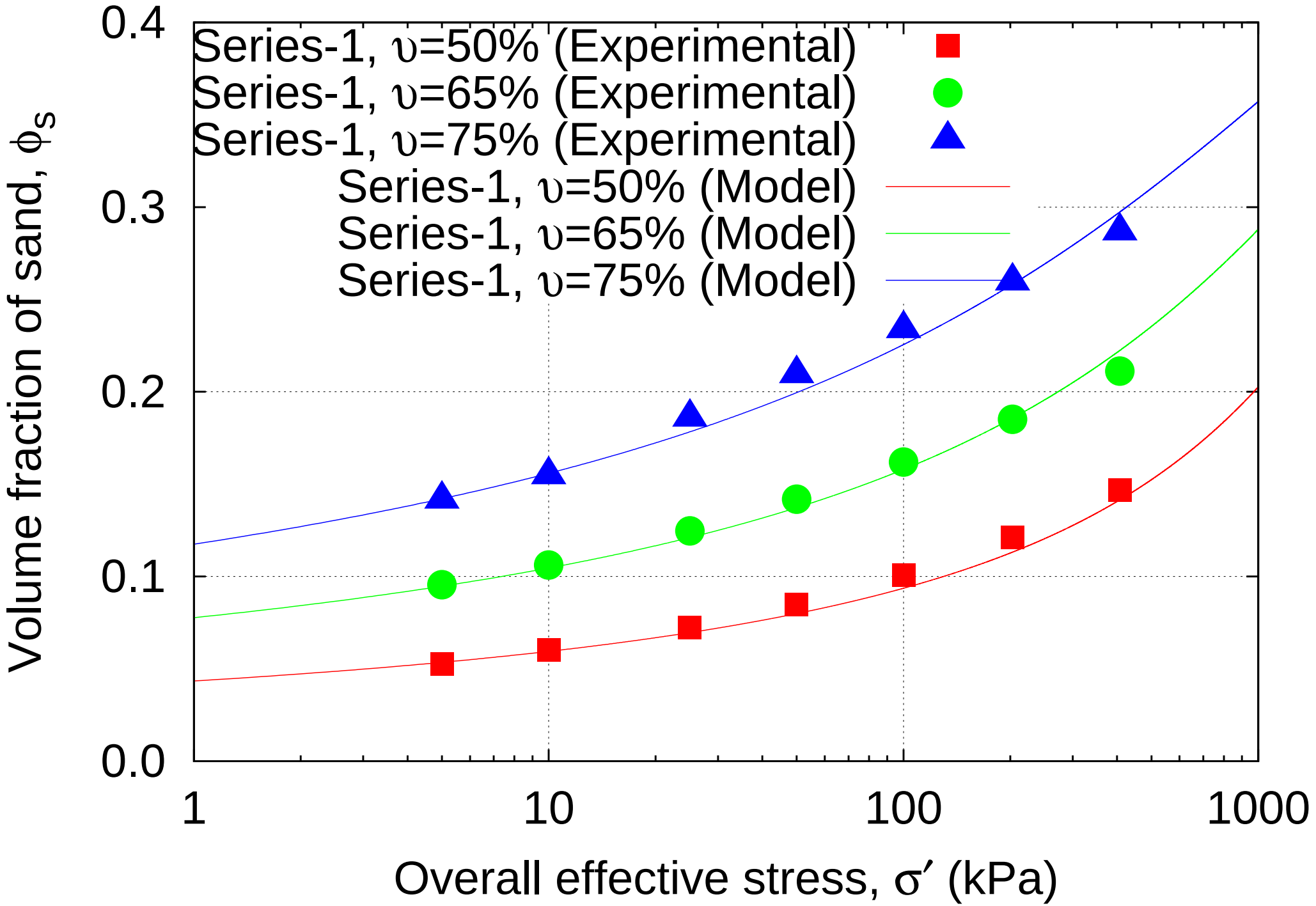

Figure14b

Click here to download Figure Figure14b.eps

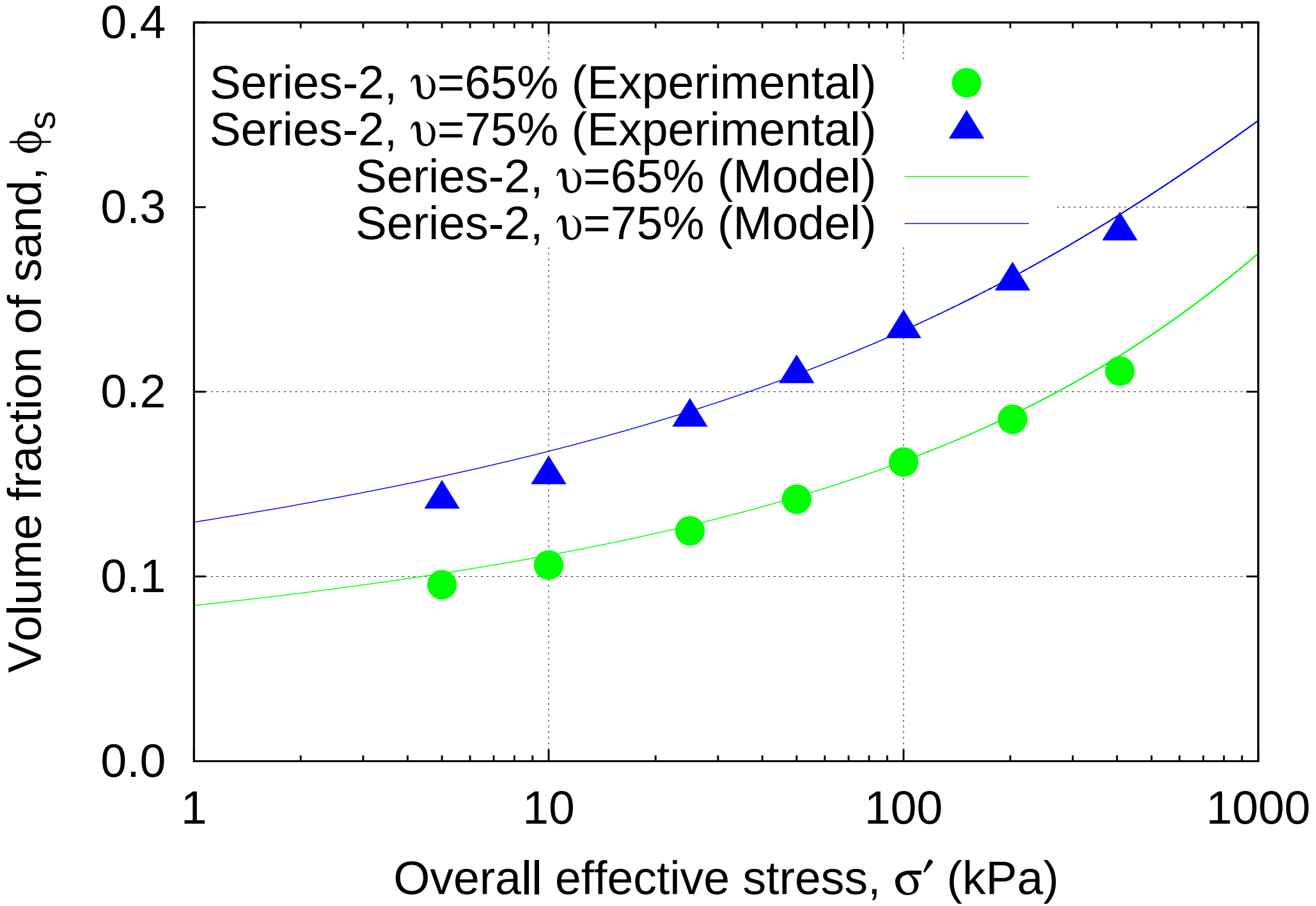

Figure15a

Click here to download Figure Figure15a.eps

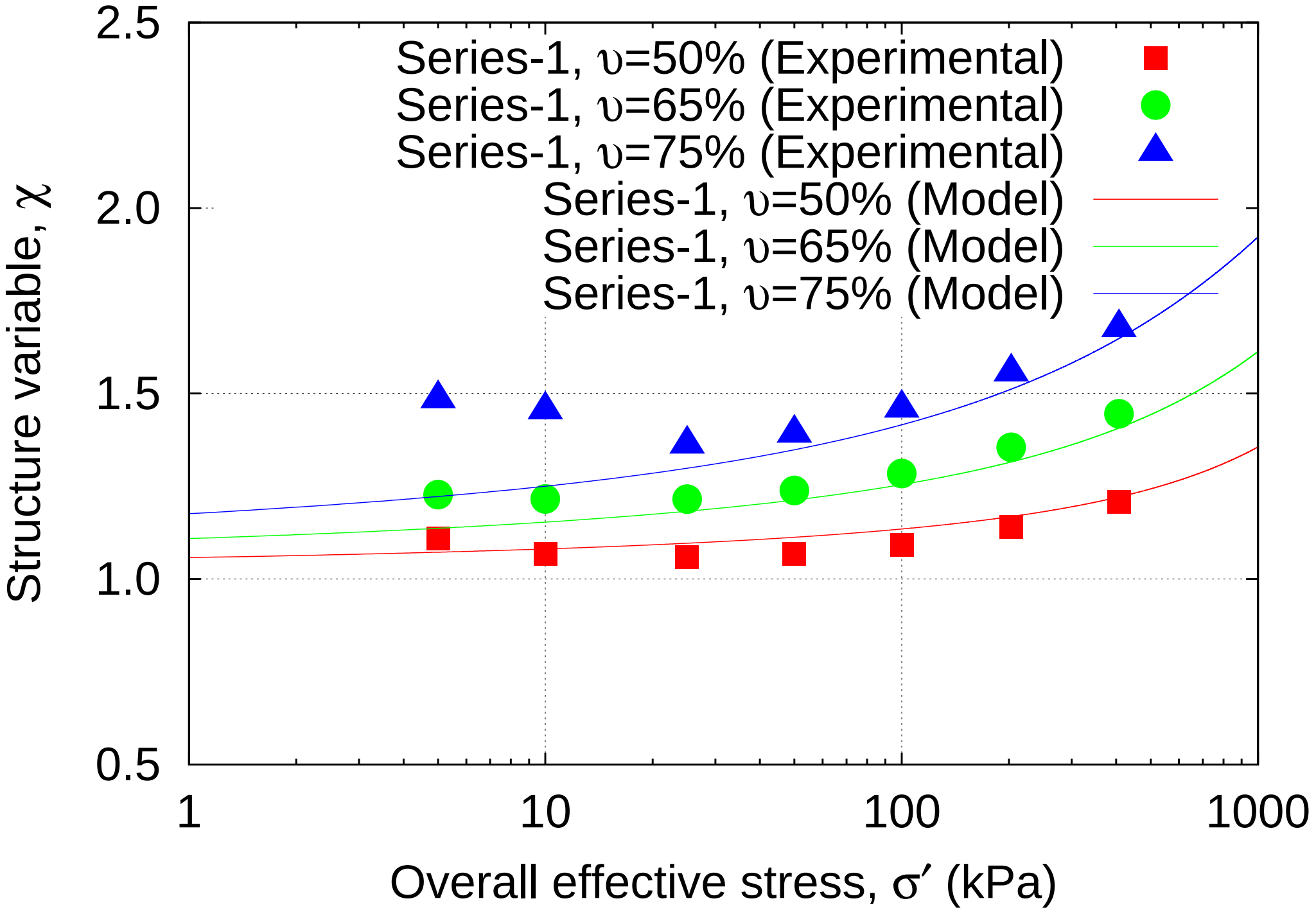

Figure15b

Click here to download Figure Figure15b.eps

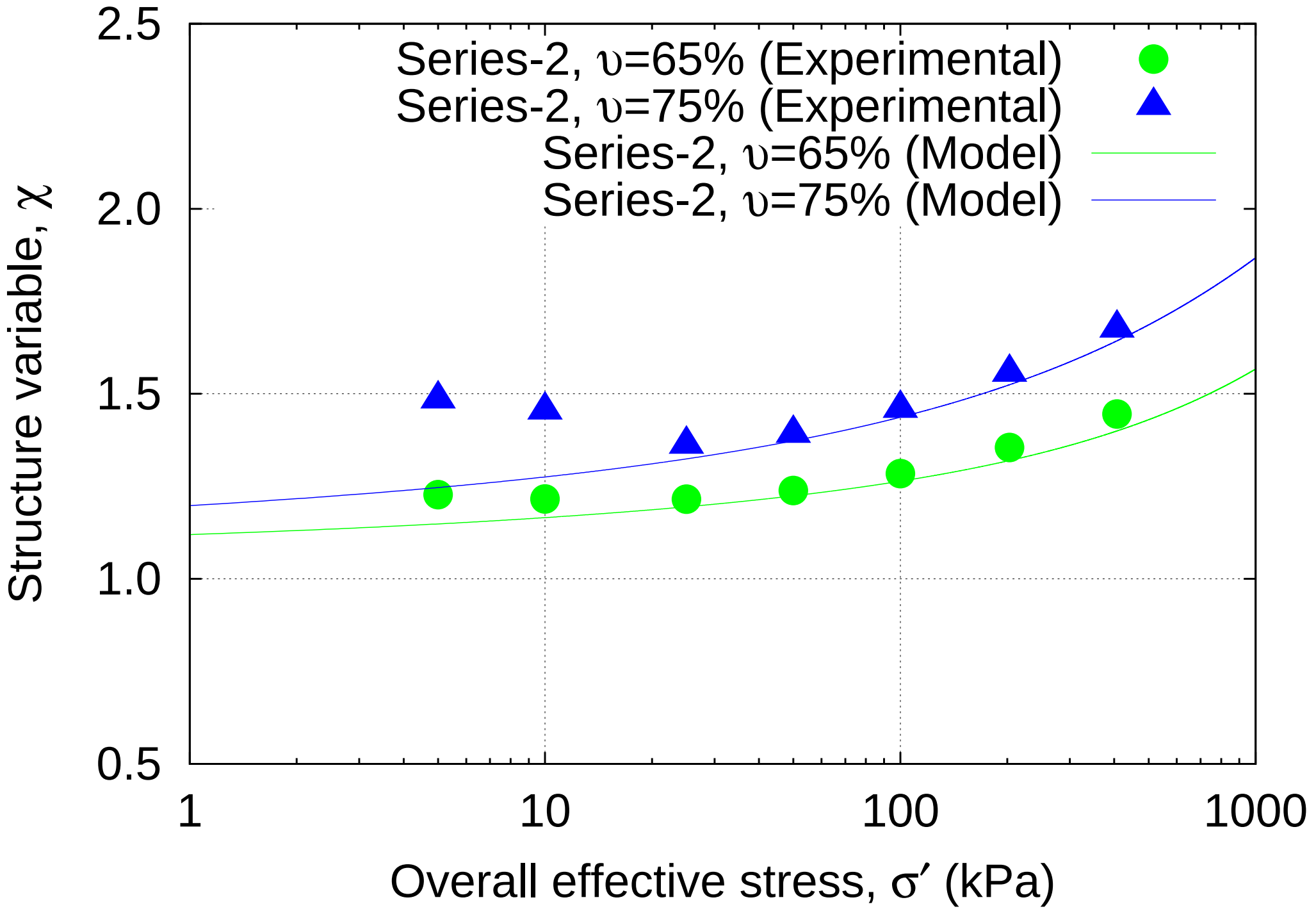

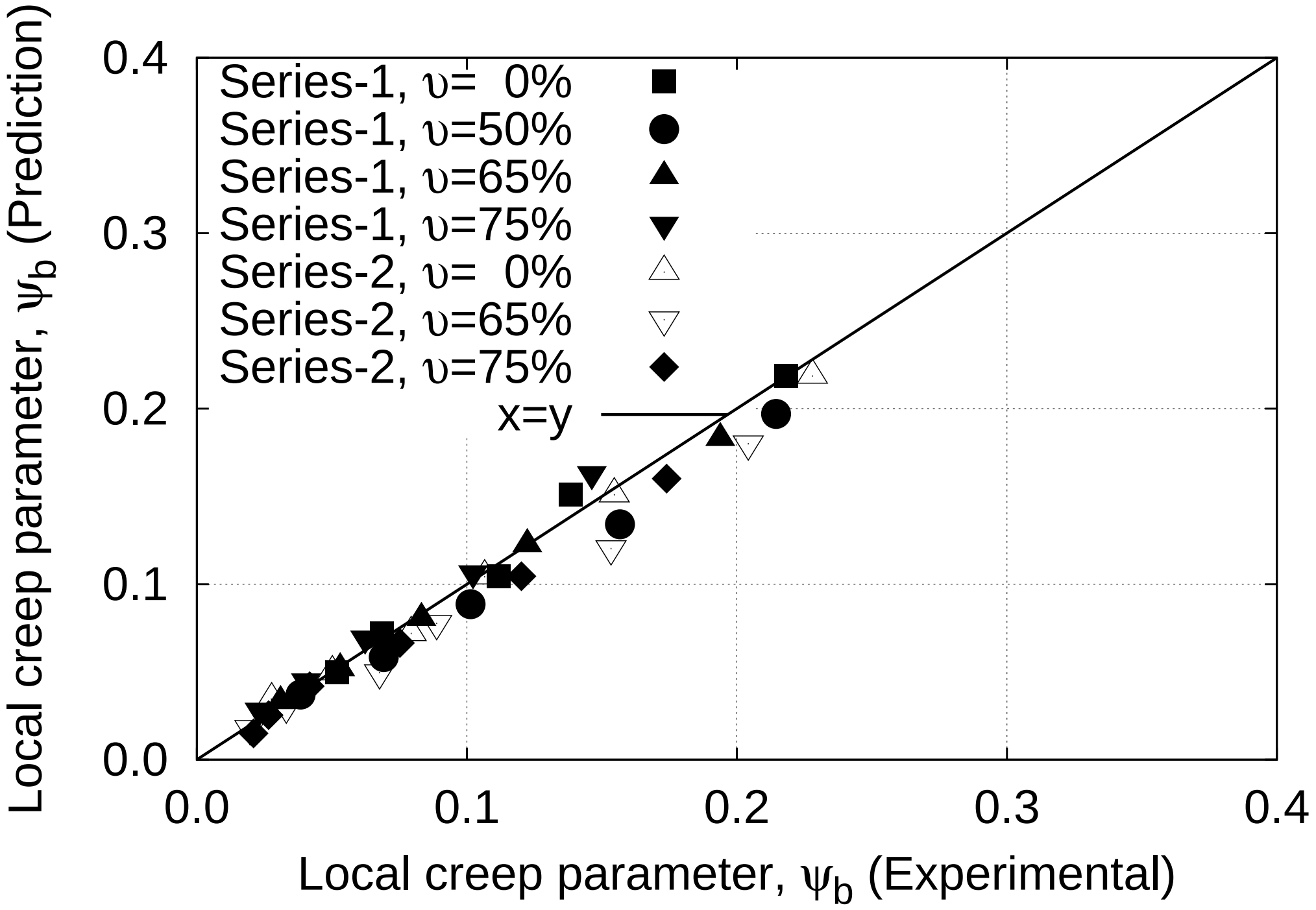

Figure17a

Click here to download Figure Figure17a.eps

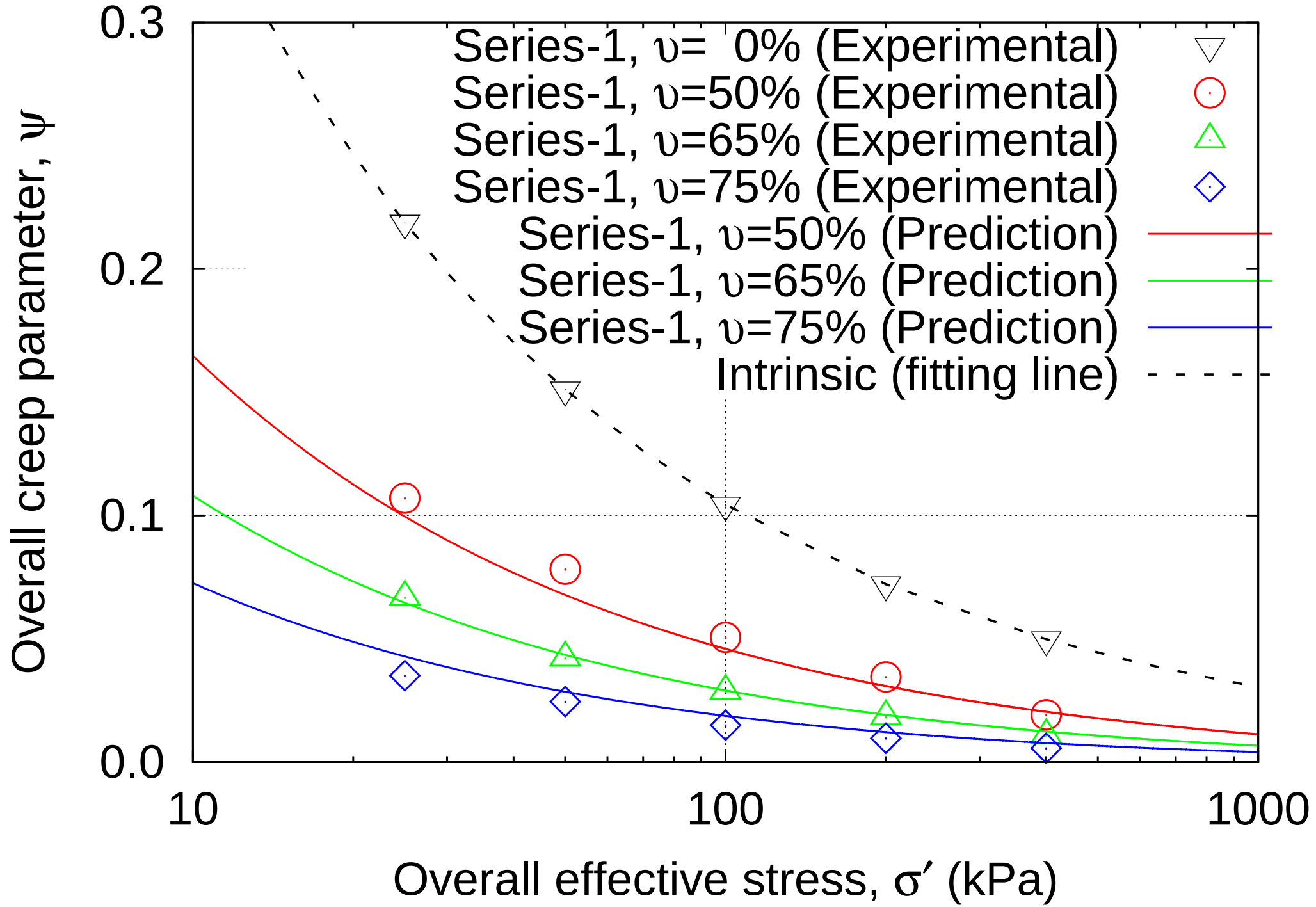

Figure17b

Click here to download Figure Figure17b.eps

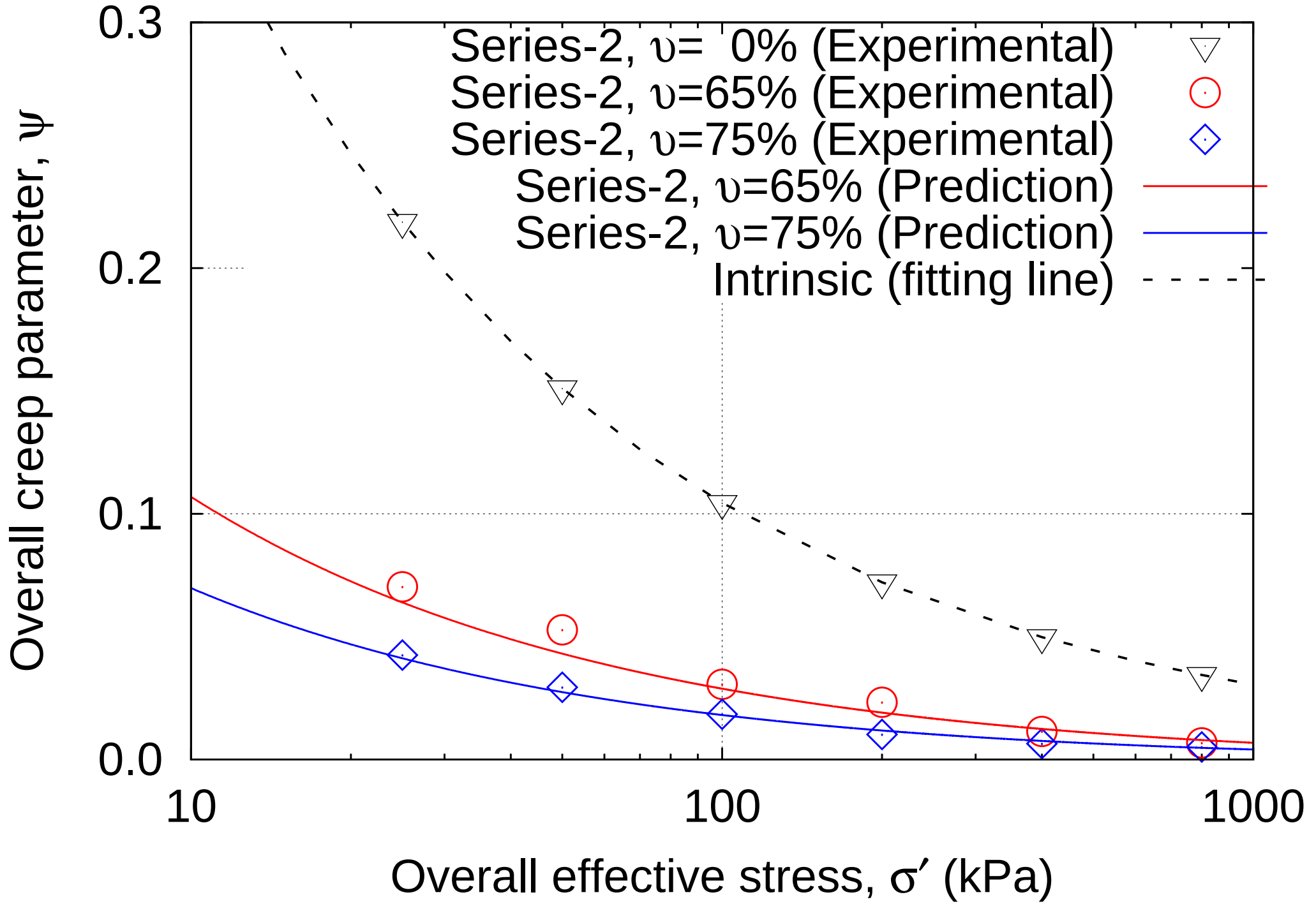

List of Figures